Pharm Res (2015) 32:910–928
DOI 10.1007/s11095-014-1506-0

RESEARCH PAPER

Dendrimer-stabilized smart-nanoparticle (DSSN) platform for targeted delivery of hydrophobic antitumor therapeutics

Rakesh K. Tekade • Muktika Tekade • Manoj Kumar • Abhay S. Chauhan

Received: 22 April 2014 / Accepted: 29 August 2014 / Published online: 10 September 2014

ABSTRACT

Purpose To formulate dendrimer-stabilized smart-nanoparticle (DSSN; pD-ANP-*f*) for the targeted delivery of the highly hydrophobic anticancer drug, Paclitaxel (PTXL).

Method The developed nanoformulations were evaluated for particle size, surface-charge, loading efficiency, particle density, *in-vitro* drug release, SEM/TEM, cytotoxicity assay, fluorescence uptake, HPLC quantitative cell uptake assay, flow cytometry, tubulin polymerization, and stability assessments.

Results The developed pD-ANP-*f* nanoformulation (135.17 ± 7.39 nm; −2.05 ± 0.37 mV and 80.11 ± 4.39% entrapment) exhibited a pH-dependent drug release; remained stable in physiological pH, while rapid releasing PTXL under tumorous environment (pH 5.5). The cytotoxicity assay performed in cervical, breast, blood, and liver cancer cell lines showed pD-ANP-*f* to be strongly suppressing the growth of cancer cells. We investigated the fluorescence based intracellular trafficking and HPLC based cellular uptake of nanoformulated drug and the result indicates higher cellular uptake of pD-ANP-*f* compared to other formulations. pD-ANP-*f* prominently induced apoptosis (73.11 ± 3.84%) and higher polymerization of tubulins (59.73 ± 6.22%). DSSN nanoformulation was found to be extremely biocompatible (<1% hemolytic) compared to naked PTXL (19.22 ± 1.01%) as well as PTXL-dendrimer nanocomplex (8.29 ± 0.71%).

Conclusion DSSN strategy is a novel and promising platform for biomedical applications that can be effectively engaged for the delivery of drug/gene/siRNA targeting.

KEY WORDS albumin · cancer cell uptake · caspase activity · dendrimer · fluorescence imaging

INTRODUCTION

The development of a suitable nanocarrier for the targeted delivery of anticancer bioactives is of growing interest in the field of applied biomedical sciences (1). Assortments of nanocarrier systems are presently being explored to accomplish this objective (2). The selection of suitable biomaterials for the preparation of nanoparticles has long been an essential consideration (3) and, in this context, negatively charged albumin represents an attractive biopolymer.

Albumin is a hydrophilic, safe, biocompatible, and biodegradable natural biopolymer (4), that has been approved by FDA for *in vivo* administration in patients (5). Several investigators have reported the formulation of albumin-based nanocarriers for the delivery of hydrophobic drug. However, most of these formulations employ co-solvent like di-methyl sulfoxide (DMSO) to load hydrophobic drug, but, low drug

Rakesh K. Tekade and Muktika Tekade having equal contribution and can be interchangeably written as first authors.

R. K. Tekade
Preclinical Nuclear Imaging Laboratory, The University of Texas Southwestern Medical Center 5323 Harry Hines Boulevard Dallas, Texas 75390, USA

R. K. Tekade (✉)
Department of Pharmaceutical Technology, School of Pharmacy, The International Medical University Jalan Jalil Perkasa 19 Kuala Lumpur 57000, Malaysia
e-mail: rakeshtekade@gmail.com

R. K. Tekade
e-mail: rakeshkumar@imu.edu.my

M. Tekade
TIT College of Pharmacy, Technocrats Institute of Technology Campus Anand Nagar Bhopal, MP 462021, India

M. Kumar
School of Medicine and Public Health, University of Wisconsin-Madison Madison, Wisconsin 53705, USA

A. S. Chauhan (✉)
School of Pharmacy, Concordia University Wisconsin Mequon, Wisconsin 53097, USA
e-mail: abhaychauhan74@gmail.com

loading as well as high drug leaching are potential limitations associated with such formulation strategies (6). In this direction, we recently reported the preparation of albumin nanoparticles using a mild gelation technique and the work demonstrated great potential for the delivery of anticancer drugs (7). However, the high negative charge of albumin nanoparticles impedes its uptake, while instability, low loading, as well as drug leaching tendency of loaded hydrophobic drugs, mandates improvement in its nanoformulation strategy (7). Herein, we propose a novel concept formulation of dendrimer stabilized albumin nanocarrier for the targeted delivery of highly hydrophobic anticancer drug, paclitaxel (PTXL).

Dendrimers represent the family of polyelectrolytes with perfectly monodisperse and regular core-shell highly branched nanostructure (size <10 nm) (8). Dendrimers have attracted widespread consideration owing to their versatile architecture. The dendrimer core offers a unique microenvironment for the entrapment of hydrophobic bioactives, while the positively charged periphery can provide binding ites to load a variety of oppositely charged hydrophilic molecules (9, 10). In our previous work, we have reported successful efficacy of dendrimer with a highly loaded hydrophobic drug (9–11). The present work further widens the application of dendrimers for preparing stable albumin nanoconstructs for the delivery of hydrophobic drug, PTXL.

The interaction of dendrimer with surfactants and supramolecular surfactant assemblies such as anionic micelle, DNA (12), lipidic layer (13), anionic liposome (14), lyotropic liquid crystalline systems (15), and lamellar phase (16) have been systematically reported. Literature also reveals the successful development of dendrimer assemblies to form thin films (17). In contrast to previous studies, which investigated the influence of dendrimer on preformed supramolecular architectures (e.g. micelles, liposomes, liquid crystals, lamellae, thin film) (16), this work presents a detailed investigation towards the formation of a self-assembled nanostructure developed on controlled electrostatic gelation of anionic bovine serum albumin [zeta potential, $\zeta = -27.73 \pm 0.81$ mV; (7)] containing fourth generation poly amidoamine (4.0 G PAMAM) dendrimer to form supramolecular nano assembly (pD-ANP-*f*; Fig. 1). We were principally interested in using the high drug loading capacity of dendrimer to load hydrophobic drugs (via hydrophobic interaction), a property that is potentially afforded by dendrimer due to its hydrophobic core (18, 19).

Folate ligand based cancer targeting is a well-known concept and folic acid can be straightforwardly conjugated to albumin nanoparticles owing to availability of abundant amine groups in albumin biopolymer (20, 21). Hence, it is envisaged to append folic acid as a model targeting ligand to attain targeted delivery following receptor mediated endocytosis, while sparing normal cells (20). It is well reported that under acidic condition, amine groups of cationic dendrimer exhibit the "proton sponge effect"(10), hence, when the formed pD-ANP-*f* nanoparticles are internalized within cancer cells, dendritic nanoconstructs will undergo protonation leading to the buffering of endosomal vesicle causing endosomal swelling and lysis (22) thereby rapidly releasing the loaded drug into the cytoplasm. This innovative formulation strategy will also help in solving the drug leakage issue commonly encountered with conventional albumin based nanoparticles (6). These dendrimer-stabilized albumin nanoparticles are especially useful for drug/gene/siRNA targeting, sustained release applications.

MATERIALS AND METHODS

Materials

PAMAM Dendrimer (4.0 generation, G) with an ethylenediamine core in methanol (20%, *w*/*w*) was purchased from NanoSynthons Inc. (Michigan, USA). Folic acid, glutaraldehyde (grade II, 25%), 1-ethyl-3-(3-dimethylaminopropyl carbodiimide hydrochloride (EDC) and Nile-red were purchased from Sigma Aldrich Co. Ltd., (Gillingham, Dorset, UK) (refer supporting informations. Dialysis membrane (Spectra/Por® 3 KDa MWCO), membrane filter (Millex pore size 0.45 μm), were purchased from Fisher Scientific UK Ltd (Loughborough, UK), while Paclitaxel was purchased from ChemieTek®, USA. Albumin and tripolyphosphate (TPP) were purchased from Amresco (OH, USA) and Strem Chemicals (MA, USA), respectively.

Triton X-100, trypan blue, Corning Transwell® polycarbonate membrane inserts (pore size 3.0 μm, membrane diameter 12 mm), and Dulbecco's Modified Eagles Medium (DMEM were purchased from (MediatechInc, VA, USA). L-glutamine, non-essential amino acid, 50 IU/ml penicillin and 50 mg/ml streptomycin, trypsin-EDTA 0.25%, were purchased from Gibco BRL, Invitrogen Paisley, UK. Heat inactivated fetal bovine serum (FBS) was purchased from Atlanta Biologicals (Lawrenceville, GA, USA). All other materials for cell culture were purchased from Invitrogen Life Technologies (Paisley, Scotland). All other chemical reagents were analytical grade and obtained from commercial sources. Deionized, 0.22 μm filtered sterile water was used throughout the experiments.

Cell culture

The Human Cervical Cancer (SiHa), Human Breast Cancer (MCF-7), Human Lung adenocarcinoma epithelial cell line (A549), blood (*Jurkat*) and Liver (*HepG2*) cancer cell lines were grown as monolayer in 75 cm^2 tissue culture flasks (Greiner Bio-one, Monrow, NC, USA) at 37°C under 5% CO_2 in DMEM, RPMI and F12K medium (Life Technologies, Grand Island, NY, USA), respectively supplemented with 10% FBS and an antibiotic anti-mycotic solution of penicillin

(5,000 U/ml), streptomycin (0.1 mg/ml) and neomycin (0.2 mg/ml) (PSN).

HPLC method for analysis of PTXL

PTXL was analyzed by HPLC technique, using Agilent 1100 Series HPLC system (UK) equipped with a Luna 5 µm, C18 column (250 mm×4.6 mm; Phenomenex, Cheshire, UK). The mobile phase consisted of an optimized mixture of MeOH:water:TFA acid::80:20:0.1, *v/v/v*, with a gradient elution at a flow rate of 1 ml/min, and UV detection at 225 nm at ambient temperature was used (23). All measurements were triplicate and results averaged for calculation.

Formulation development of dendrimer stabilized albumin nanoparticles and folate anchoring

The formulation of dendrimer complexed albumin nanoparticles was achieved by a three-step process as depicted in Fig. 1. Briefly, PTXL (5 mg) and 4.0G (15 mg) dendrimer were dissolved in methanol and stirred using a magnetic bar at 300 rpm in dark at room temperature for 24 h. The solvent was then removed under vacuum followed by addition of sufficient phosphate buffer (pH 7.4) to prepare a 2%*w/v* solution. This solution was then added drop-wise (1 ml, at 0.2 ml/min) under constant stirring at 500 rpm to 1%*w/v* aqueous albumin solution (10 ml) and the resultant mixture was stirred continually at 37°C for 2 h in dark. To this mixture ethanol was added drop-wise to produce albumin nanoparticles containing drug-dendrimer complex. The resultant nanoparticles were stabilized by addition of glutaraldehyde as cross linking agent (1 µg glutaraldehyde/mg albumin) to yield stable PTXL-dendrimer complex containing albumin nanoparticles (pD-ANP). Finally, the nanoparticles were collected by centrifugation (16,000 g, 30 min), washed with PBS pH 7.4 (× 3); and the resultant product was lyophilized using 2%*w/v* lactose as cryoprotectant (24). Following conventional methodology, albumin nanocarriers (p-ANP) were also prepared (6) to assess the change in bio-performance of nanocarriers with and without inclusion of dendrimer in the formulation of ANP. The formulation of dendrimer-stabilized folate-anchored albumin nanoparticles (pD-ANP-*f*) was achieved by well-established carbodimide methodology as reported earlier by our group (9, 25) with slight modifications (see supporting information).

Formulation of dendrimer-stabilized folate-anchored albumin nanoparticles (pD-ANP-f)

The folate tagging of albumin nanoparticles was achieved by well-established carbodimide methodology as reported earlier by our group (25, 26) with slight modifications. Briefly, the carboxy group of folic acid (4 mM) was activated by adding EDC (5 mM, 25% molar excess) and stirring it for 4 h in dark. The activated folic acid is then added drop wise to the solution of pD-ANP (27) to prepare pD-ANP-*f*. The product was purified by dialysis against 1,000 ml of phosphate buffer (pH 7.4) using dialysis bag (MW cut off 5 KDa) to remove the free folic acid, EDC and other impurities from reactants. During this purification process, external buffer was replaced with fresh buffer and periodically assayed spectrophotometrically to determine the existence of free folic acid, EDC or any other impurities (un-reacted reactants) (27). Similar protocol was followed to prepare folate conjugated conventional albumin nanoparticles (p-ANP-*f*). The pD-ANP-*f* and p-ANP-*f* formulations were then lyophilized using 2% lactose as cryoprotectant, characterized as follows and stored for future studies.

Preparation of freeze dried powders containing dendrimer stabilized nanoparticles

Suspension of ANP and dendrimer stabilized ANP (pD-ANP) nanoparticles were freeze dried employing 2% *w/v* lactose monohydrate as a cryoprotectant following reported protocols (28) with slight modifications. Briefly, nanosuspension formulation in 2%*w/v* lactose monohydrate was frozen to −80°C in Ultra-Low Temperature Freezers (Thermo Fisher Scientific Inc., PA, USA) for 3 h. The frozen suspension was lyophilized for 48 h under vacuum at <0.133 mBar pressure at −84°C using a laboratory scale Freezeone 12 Plus Lyophilizer (Labconco, Kansas City, MO, USA). The nanoformulation suspension was prepared by suspending the lyophilized formulation in deionized water for further characterization. The resultant freeze dried powders were collected and stored in a desiccator at room temperature until use. The yield of freeze drying process was determined via gravimetric analysis by establishing a comparison between the weights of resultant freeze dried powder and that of the total solids involved in the formulation (29), as per following formula ($n=3$):

$$\%\textbf{Yield}(\textbf{Freeze drying Process}) = \frac{\text{Weight of nanoparticles}}{\text{Total solids (Lactose + BSA) weight}} \times 100$$

Size, surface charge and morphology of various ANP formulations

The particle size and surface charge (zeta potential) of conventionally prepared p-ANP, pD-ANP, p-ANP-*f* and pD-ANP-*f* were determined by dynamic light scattering using a NICOMP ZLS 380 analyzer (PSS-NICOMP, Santa Barbara, USA) as described previously by our group (24). The particle size and zeta potential were determined by dispersion of the prepared formulations in PBS at 25°C. All measurements were recorded in triplicate and results expressed as mean±

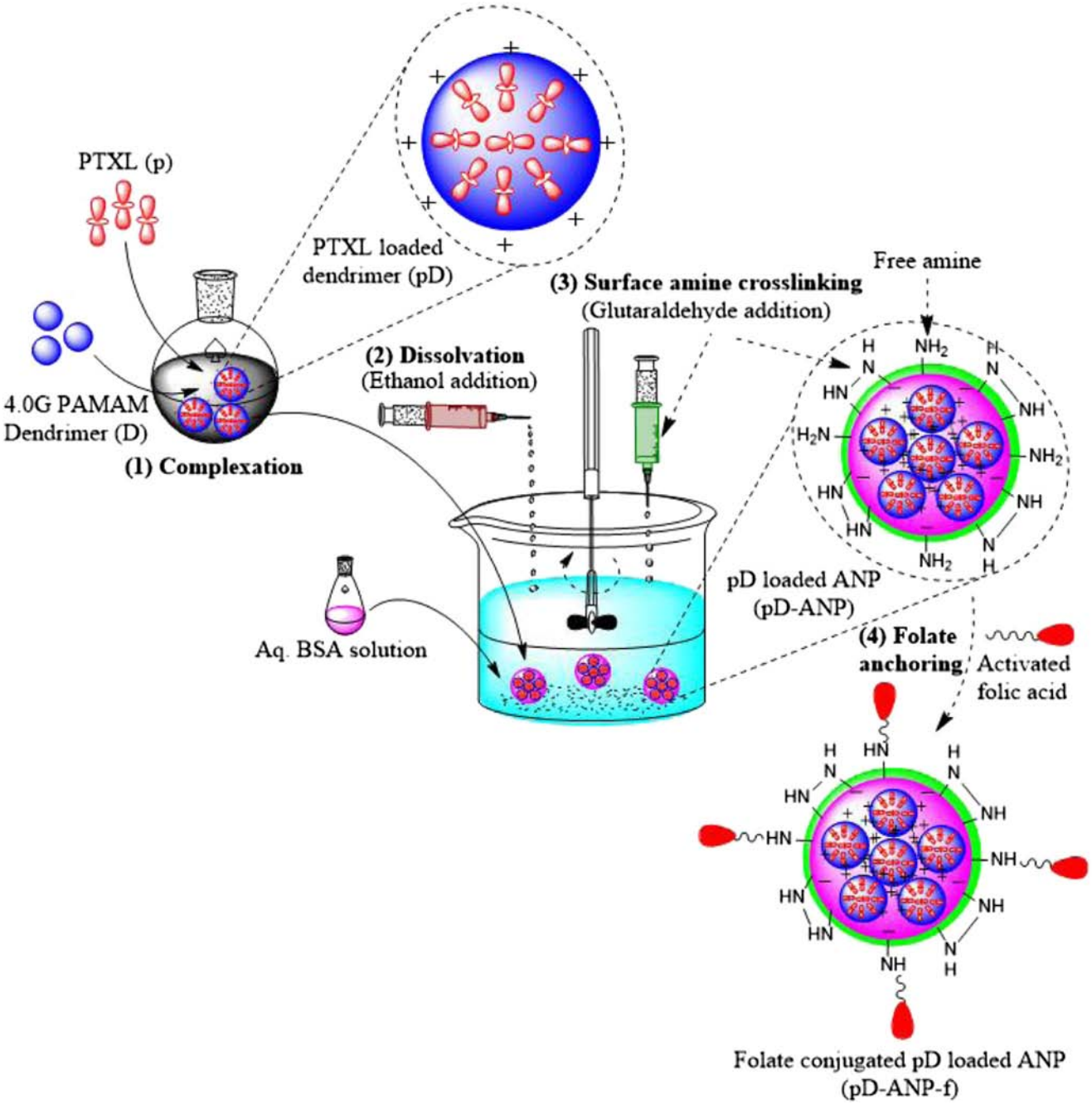

Fig. 1 Schematic showing formulation development of dendrimer stabilized- folate targeted- albumin nanoparticle (pD-ANP-*f*).

SD. The surface morphologies of p-ANP, pD-ANP, p-ANP-*f* and pD-ANP-*f* were also examined by scanning electron microscopy (SEM, LEOSUPRA 55 Genesis 2000, CarlZeiss, Germany) and transmission electron microscope (TEM, Hitachi H-7600, Japan).

Determination of entrapment efficiency

Entrapment efficiency was determined by employing Vivaspin-500 ultracentrifuge filters with molecular cut off weight of 100 K.Da (Viva Products, Inc., Littleton, MA, USA). Briefly, PTXL loaded formulation (0.5 ml) was placed in Vivaspin500 ultracentrifuge tubes with filter membranes (molecular weight cutoff 300 K Da) and centrifuged at 13,000 rpm for 15 min. The aqueous filtrate generated at the bottom of Vivaspin500 ultracentrifuge tubes was subjected to HPLC analysis to determine the concentration of loaded and free PTXL. The entrapment efficiency (EE) of the PTXL within developed formulations was defined as the drug content and was calculated by employing equation (1).

$$\%\textbf{Entrapment Efficiency}(\textbf{EE}) = \frac{X_1 - X_2}{X_1} \times 100 \qquad (1)$$

Where,

X_1 Amount of total PTXL taken (mg).
X_2 Amount of free/leaked PTXL detected in supernatant after ultracentrifugation (mg).

In-vitro release of PTXL from various nanoformulation

In-vitro release of PTXL from the developed formulations (p-ANP, pD-ANP, p-ANP-*f* and pD-ANP-*f*) were evaluated using extensive dialysis technique (9, 10, 26). Briefly, drug-loaded formulation was placed into a pre-swollen dialysis cassette (molecular weight cutoff of 12 K Da; Sigma, USA) and immersed in a glass vessel containing 500 ml of PBS (pH 5.5 or 7.4) with 1%*v/v* PEG 4000. The entire drug release assembly was maintained at 37 ± 2°C with continuous slow magnetic stirring at 300 rpm. At predetermined time intervals (0.25, 0.5, 1, 2, 4, 6, 8, 12, 24 and 48 h), 1 ml aliquots were withdrawn from the dissolution medium and replenished with same volume of fresh medium to preserve the sink condition. The samples were analyzed at each time point using the HPLC method as described above (23), and the release profile was created by plotting time (x-axis) versus cumulative percent PTXL release (y-axis).

Differential scanning calorimetry

The nanoformulations were also characterized by differential scanning calorimetry (DSC) using a DSC1 instrument (Mettler Toledo, Columbus, OH, USA). For this study approximately two mg of different samples were placed into an aluminum pan separately and a lid was hermetically sealed. The pan was then positioned in the analyzing cell of a DSC module and the temperature of the DSC module, equilibrated at 35°C and the thermal behavior was determined by amplifying the temperature at a rate of 10°C/min under N_2 environment until the sample began to degrade. Baselines were determined using an unfilled pan, and all the thermograms were corrected for baseline. Transition temperatures were determined from the endothermic peak minima while transition enthalpies were obtained by integration of the endothermic transitions using linear baselines.

pH stability studies

Nanoformulations (p-ANP, pD-ANP, p-ANP-*f* and pD-ANP-*f*) were also exposed to varying pH conditions to infer the effect of pH on size and charge of developed targeted formulations. For this investigation, pH 7.4 and 5.4 were selected to assess the stability of formulation under physiological conditions (blood) and acidic tumor environment, respectively (30).

Hemolytic activity

The study was performed following protocol reported earlier with slight modifications (31). Briefly, RBCs were collected from human blood and re-suspended in normal saline to get 5% RBC suspension. To 1 ml of RBC suspension 5 ml distilled water as well as 5 ml normal saline were added separately, which were considered to be 100% and 0% hemolytic, respectively. Similarly, formulations such as plain PTXL, p-ANP, pD-ANP, p-ANP-*f* and pD-ANP-*f* (0.5 ml) were added separately to a mixture of normal saline (4.5 ml) and RBC suspension (1 ml). All the sample tubes were allowed to stand for 30 min with mild shaking intermittent and were centrifuged for 15 min at 3,000 rpm in an ultracentrifuge. The supernatants were analyzed by UV spectrophotometric assay (1601 UV–Visible spectrophotometer, Shimadzu, Japan) at 540 nm and the degree of hemolysis was determined by the following equation:

$$(\%)\text{Hemolysis} = \frac{\text{Abs} - \text{Abs}_0}{\text{Abs}_{100} - \text{Abs}_0} \times 100$$

Where Abs, Abs_0 and Abs_{100} are the absorbance of samples, a solution of 0% hemolysis, and a solution of 100% hemolysis, respectively.

MTT cytotoxicity assay

The *in vitro* cytotoxicity of free PTXL as well as developed formulations (p-ANP, pD-ANP, p-ANP-*f* and pD-ANP-*f*) were evaluated by *MTT* cytotoxicity assay based on measurement of the activity of enzymes present in live cells that reduces *MTT* to give a purple color formazan (10). This assay was performed on five Cervical (*SiHa*), Breast (*MCF-7*), Lung (*A549*), blood (*Jurkat*) and Liver (*HepG2*) cancer cell lines. Briefly, cells (5×10^3) were seeded evenly into 96-well flat-bottomed tissue culture plate (Iwaki; Japan) in medium (Mediatech Inc, VA, USA) supplemented with 10%*v/v* FBS (FBS; Sigma, USA) and 1%*v/v* Penicillin-Streptomycin mixture (Sigma, USA). The cells were incubated for 24 h in a humidified atmosphere of 5% CO_2 at 37 ± 0.5°C and treated with freshly prepared formulations as standard solutions between 0.001 and 100 μM concentrations. After 24 h, 20 μl *MTT* (5 mg/ml) in PBS (pH 7.4) was added to each well and the plate was incubated for 2 h at 37 ± 0.5°C, allowing viable cells to reduce the *MTT* into purple colored formazan crystals. The formazan crystal was dissolved by adding 100 μl of Lysin-buffer (TrisHCl, 10 mM; NaCl, 75 mM; EDTA, 10 mM; Sodium dodecyl sulphate, 0.5% in water) containing

Proteinase-K (0.15 mg/ml). The absorbance was measured at 570 nm using ELISA microplate reader (Synergy H1, Bio-Tek, USA) at 37±0.5°C.

Fluorescence and HPLC based cell uptake assay

Human breast cancer cell line (MCF-7) was selected for this investigation due to its stable and comparatively larger morphology. Briefly, MCF-7 cells were seeded on six well plates (5×10^4/well) and incubated at 37±0.5°C under 5% CO_2 for 24 h. After 24 h media was removed, and incubated with 2 ml of FITC tagged formulations (^{FITC}p-ANP, ^{FITC}pD-ANP, ^{FITC}p-ANP-*f* and ^{FITC}pD-ANP-*f*) for 1 h. After 1 h, media was removed; cells were washed with PBS (×3) and fixed with 2% formaldehyde for 10 min, followed by washing with PBS twice. The samples were imaged using Axiovert 40 CFL inverted microscope (Carl Zeiss Microscopy, LLC, USA) at 40× magnification with FITC excitation and emission spectrum peak wavelengths of 495 nm and 519 nm respectively with an Exfo X-Cite series 120 mercury vapor lamp as light source for fluorescence imaging (Lumen Dynamics Group, Inc., Mississauga, Ontario, Canada).

In order to determine the time bound quantitative cellular uptake of the PTXL in MCF-7 cells following treatment of various nanoformulations, HPLC analysis of cell associated PTXL was also done employing methods recently reported by our group (23). Briefly, MCF-7 cells were seeded on six well plates (5×10^5/well) and incubated at 37±0.5°C under 5% CO_2 for 24 h. After 24 h media was removed, and incubated with 2 ml of PTXL formulations (p-ANP, pD-ANP, p-ANP-*f* and pD-ANP-*f*) for 1, 2, 4 and 6 h. After incubation of cells for predetermined intervals of time, media was removed; washed thrice with PBS and treated with 100 µL trypsin PBS solution (2.5 mg/ml) and further incubated for 10 min and then harvested by adding 400 µL TBME:DEE::50:50*v*/*v* as extraction media selected as per method recently developed by us (23). The cell lysate was centrifuged at 10,000 rpm for 15 min and the PTXL content was measured by HPLC.

Flow cytometry assay

Assay was performed to assess the destiny of cells following treatment of various formulations. For this investigation MCF-7 cells were selected on ground of intermediate level of folate expression on MCF-7 cells (32) and its robust life cycle and sturdy morphology that help in nullifying effect of auto cell-death and apoptosis (33). Briefly, *MCF-7* cells were either left untreated (control) or treated with 100 nM PTXL equivalent p-ANP, pD-ANP, p-ANP-*f* and pD-ANP-*f* formulations for 6 h. Cells were then incubated with Annexin V-FITC in a buffer containing Propidium Iodide (PI) and analyzed by flow cytometry (Becton Dickinson, USA). Untreated (Annexin V-FITC and PI negative) cells, represents viable cell population those are not undergoing any apoptosis/necrosis (34, 35). Flow cytometry was performed on single-cell suspensions of adherent human breast cancer cell line, *MCF-7* (after trypsin and EDTA treatment) by subjecting to FACS analysis using FACS ARIA (Becton Dickinson, USA) (36).

Cell apoptosis assay

For this assay, MCF-7 cells were seeded on the 24 well plates (5×10^4/well), incubated at 37±0.5°C under 5% CO_2 for 24 h and treated with various PTXL nanoformulations (p-ANP, pD-ANP, P-ANP-*f* and pD-ANP-*f*) for 24 h. Untreated cells were used as a control. At the end of the incubation, the cells were trypsinized, cell pellet was collected and resuspended in 100 µl cell lysis buffer. The cell lysate was centrifuged at 10,000 rpm for 15 min and the protein concentration in the supernatant was determined employing BCA assay kit (Pierce). After this, 50 µl of buffer solution supplemented with 5 mM DTT was added to reaction mixture and incubated at 4°C. The substrate DEVD-pNA was added to each tube (10 µl, 50 µM) and incubated for 2 h at 37°C. The sequence DEVD is based on caspase-3 cleavage site in poly (ADP-ribose) polymerase (PARP) and the associated caspase activity can be quantified by spectrophotometric detection of free substrate p-nitroanilide (pNA, λ_{max} 405 nm) after cleavage from the peptide substrate DEVD-pNA, using Microplate reader

Tubulin polymerization assay

The assay was done following established protocol for the determination of levels of tubulin polymerization (37). Briefly, MCF-7 cells plated on six-well plates (5×10^5 cells/well) were treated with various PTXL formulations as described above and incubated for 1 h at 37±0.5°C. The cells were then washed and lysed using 150 µL hypotonic buffer solution (2 mM EGTA, 1 mM $MgCl_2$, 2 mM phenylmethylsulfonyl fluoride, 10 µL/mL protease inhibitor, 20 mM Tris HCl), incubated in the dark (37±0.5°C, 15 min) and then transferred to a micro centrifuge tube by cell scraping. The micro centrifuge tubes were then centrifuged at 18,000*g* for 15 min, and the polymerized tubulin was collected as sediment pellet. Protein fractions in the supernatant and the pellet were resolved by SDS-PAGE electrophoresis and then transferred to membranes, which were probed with a monoclonal antibody to α-tubulin (Sigma Aldrich, MO, USA). Level of tubulin was then determined by densitometry using Quantity One software (Bio-Rad) and the amount of polymerized tubulin was calculated by dividing the densitometric value of polymerized tubulin fraction (insoluble fraction) by the sum of polymerized and soluble fractions for each treatment group, and the results were expressed as a percentage insoluble polymer fraction (37, 38).

Statistical analysis

The experiments were conducted in triplicate unless specified, and the data presented as mean ± standard deviation. A one-way analysis-of-variance (ANOVA) with Tukey's multiple comparison post-test was used in the analysis of differences between the physicochemical properties of nanocarriers. The differences were considered to be significant at $p<0.05$. The least significant difference post-hoc ANOVA-analysis was used in the comparison of biopharmaceutical properties of different formulations.

RESULTS

Particle size

Dendrimer stabilized albumin nanoparticles (pD-ANP) were successfully prepared as briefed in proposed methodology (Fig. 1), with particle size of 89.38 ± 5.62 nm as against to conventional prepared albumin nanoparticles (p-ANP) of size 75.25 ± 6.91 nm. Analogous observations were noted in case of folate anchored counterparts of p-ANP (i.e. p-ANP-*f*) and pD-ANP (i.e. pD-ANP-*f*), wherein, p-ANP-*f* and pD-ANP-*f* showed particle size of 115.72 ± 8.69 nm and 135.17 ± 7.39 nm, respectively (Fig. 2).

Surface morphology and surface charge

SEM and TEM photomicrograph of selected ANP's were taken to assess its structure as well as surface topography. SEM pictures inferred formulations to be rounded and nanometer in size. pD-ANP-*f* was found to be more rounded and uniform in terms of their shape-size as compared to conventionally driven p-ANP-*f* formulations (Figs. 2 and 3). The formulation of conventional technique driven p-ANP's showed average surface charge of −23.05 ± 1.08 mV, while pD-ANP formulation showed significantly lower ($p<0.005$) surface charge of −5.68 ± 0.95 mV. Similar observation was made in case of p-ANP-*f* and pD-ANP-*f* formulations, wherein surface charge of −19.86 ± 2.83 mV and −2.05 ± 0.37 mV, respectively were observed.

Entrapment efficiency

The entrapment efficiency of PTXL was found to be 59.08 ± 3.85% and 57.75 ± 6.83% with p-ANP and p-ANP-*f*, while higher entrapment of 79.85 ± 8.01% ($p<0.005$) and 80.11 ± 4.39% ($p<0.005$) was observed with pD-ANP and pD-ANP-*f*, respectively (Fig. 4a–c).

In vitro drug release studies

In vitro release of PTXL from various nanoformulations was studied at pH 7.4 and pH-5.4 to assess PTXL release under physiological conditions (blood) and acidic tumor environment, respectively. The outcome of the investigation clearly inferred slow-sustained and pH responsive drug release patterns from all the nanoformulations compared to plain PTXL (Fig. 5a–b). Close examination of release data infer that PTXL release was significantly lower ($p<0.05$) in case of dendrimer stabilized ANP's. Plain PTXL formulation released more than half of the loaded drug (51.07 ± 3.12%) in merely 1 h, while at the same time point, p-ANP and p-ANP-*f* released 22.15 ± 1.84% and 17.08 ± 0.97% drug, respectively. It should be noted that corresponding dendrimer stabilized formulations (pD-ANP and pD-ANP-*f*) released significantly low percentage of drug (5.96 ± 0.21% and 2.37 ± 0.08%, respectively) at 1 h time point. At 24 h time point, p-ANP and p-ANP-*f* released 71.13 ± 4.82% and 66.39 ± 6.02% PTXL, respectively, while, the corresponding modified pD-ANP and pD-ANP-*f* formulations released 55.52% and 47.06 ± 3.18% PTXL, respectively. Similar trend of drug release was observed till the end of study, concluding the inclusion of dendrimer as an effective strategy for the ANP formulation.

The slow *in vitro* release of PTXL from p-ANP-*f* and pD-ANP-*f* can be attributed to stearic hindrance offered by folic acid residue conjugated on the surface of nanocarrier. The outcomes of this study was in agreement with earlier investigations wherein impeded drug release (upto 35% lower release) was observed in case of folate modified nanocarriers compared to unmodified nanocarrier counterpart (39,40). Chandrasekari *et al.* have also compared the influence of number of folic acid conjugated to nanocarrier on drug release, wherein nanocarrier with higher folic acid (20.1 folate per nanocarrier) exhibited approximately 15% low indomethacin release compared to intermediate folate (11.92 folate per nanocarrier); and approximately 25% low indomethacin release compared to low (3.86 folate per nanocarrier) folate modified nanocarrier (39).

Differential scanning calorimetry

DSC is a thermoanalysis method for measuring the temperature and heat flow associated with transitions in materials as a function of time. DSC analysis was performed to assess the thermal stability and transformation in nature of sample over a range of temperatures. For this investigation, free PTXL, free folic acid, BSA, PAMAM, pD-ANP and pD-ANP-*f* were studied and compared. The existence of shifted as well as narrower peaks of PAMAM and PTXL in case of pD-ANP confirmed formation of PTXL-PAMAM coupled loaded nanoconstruct. Similarly, presence of lifted peaks of PAMAM, PTXL and folic acid in case of pD-ANP-*f*

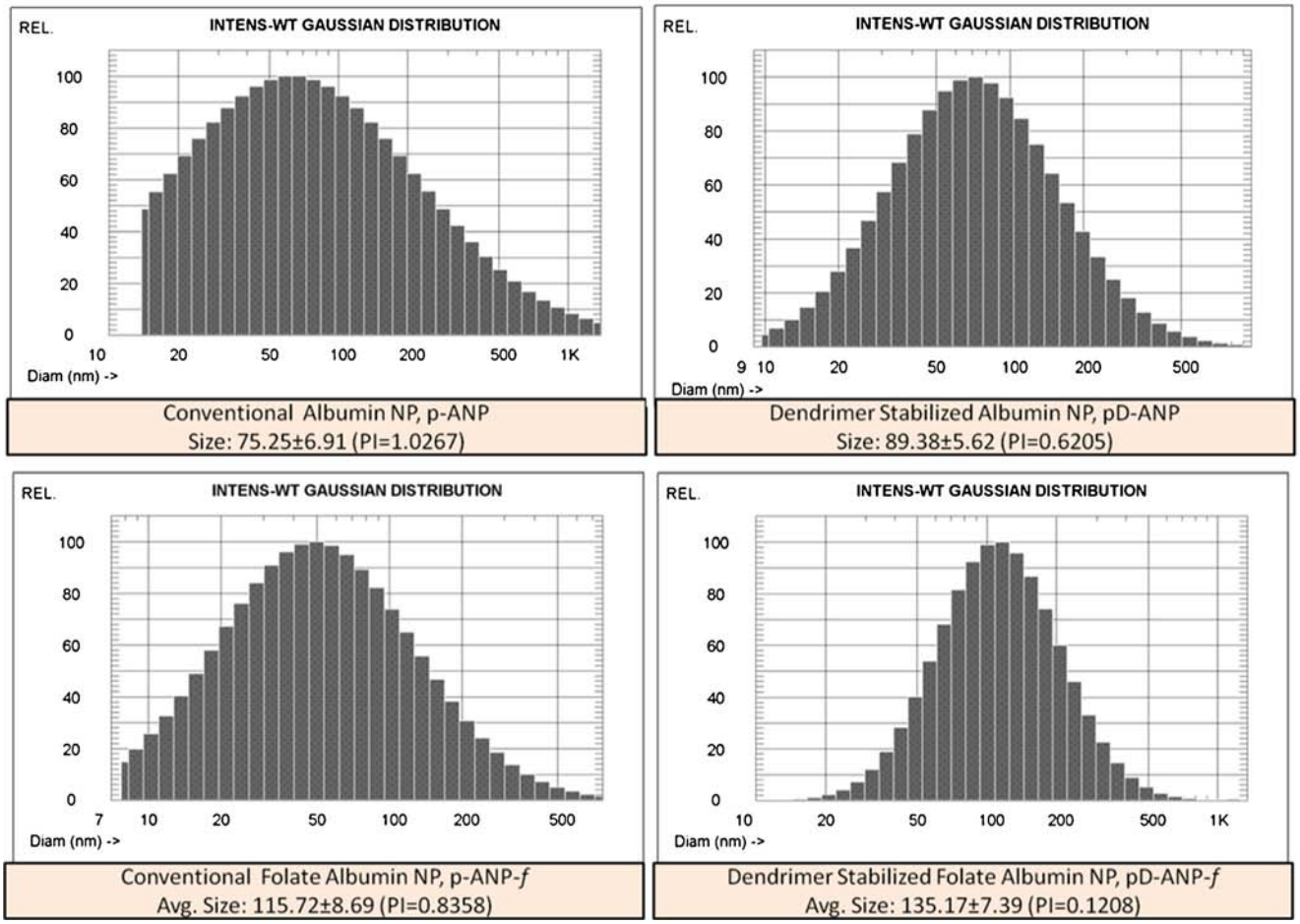

Fig. 2 Particle size distribution of (**a**) p-ANP, (**b**) pD-ANP, (**c**) p-ANP-*f*, and (**d**) pD-ANP-f. *p*-ANP and p-ANP-f represents PTXL loaded non-targeted as well as folate targeted ANP's, respectively, formulated using conventional method. On the other hand, pD-ANP and pD-ANP-f represents dendrimer stabilized non-targeted and folate conjugated ANP's formulated using method modified methodology. Particle size and polydispersity index was determined in PBS at 25°C by dynamic light scattering using a NICOMP ZLS 380 analyzer (PSS-NICOMP, Santa Barbara, USA. Results are represented as mean ± SD ($n = 3$).

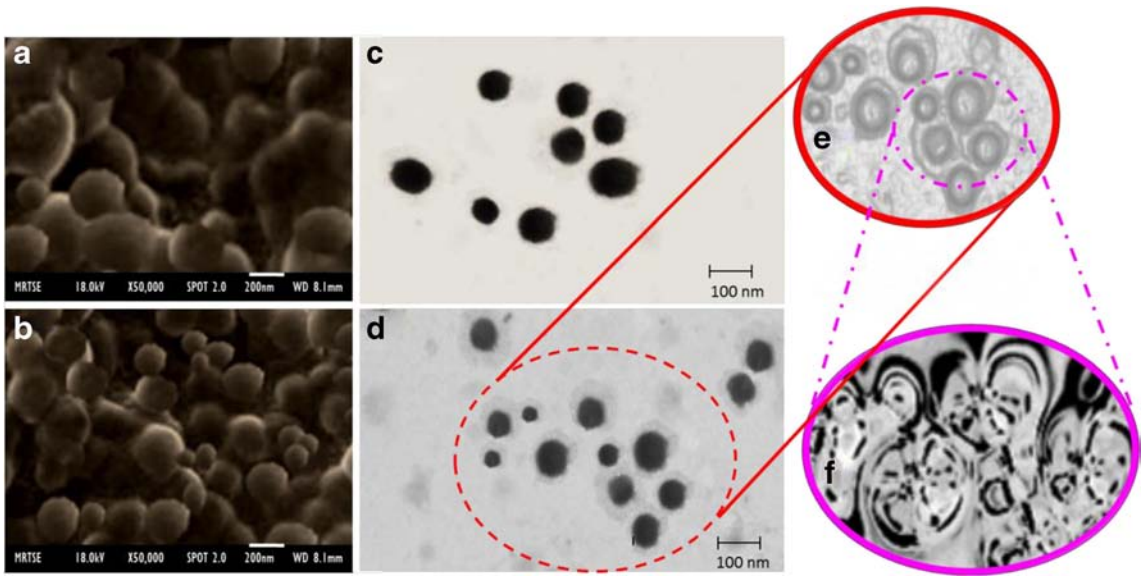

Fig. 3 SEM photomicrograph of (**a**) p-ANP-*f* and (**b**) pD-ANP-*f* at a magnification of X2000; (**c**) and (**d**) represents TEM photomicrograph of p-ANP-f and pD-ANP-*f*, respectively at an acceleration voltage of 80 KV and X200K magnification. Insat (**e**) and (**f**) represents transmission electron microscopy photomicrograph of pD-ANP-*f* at an acceleration voltage of 120 KV/X200K and 120 KV/X250K magnification, respectively.

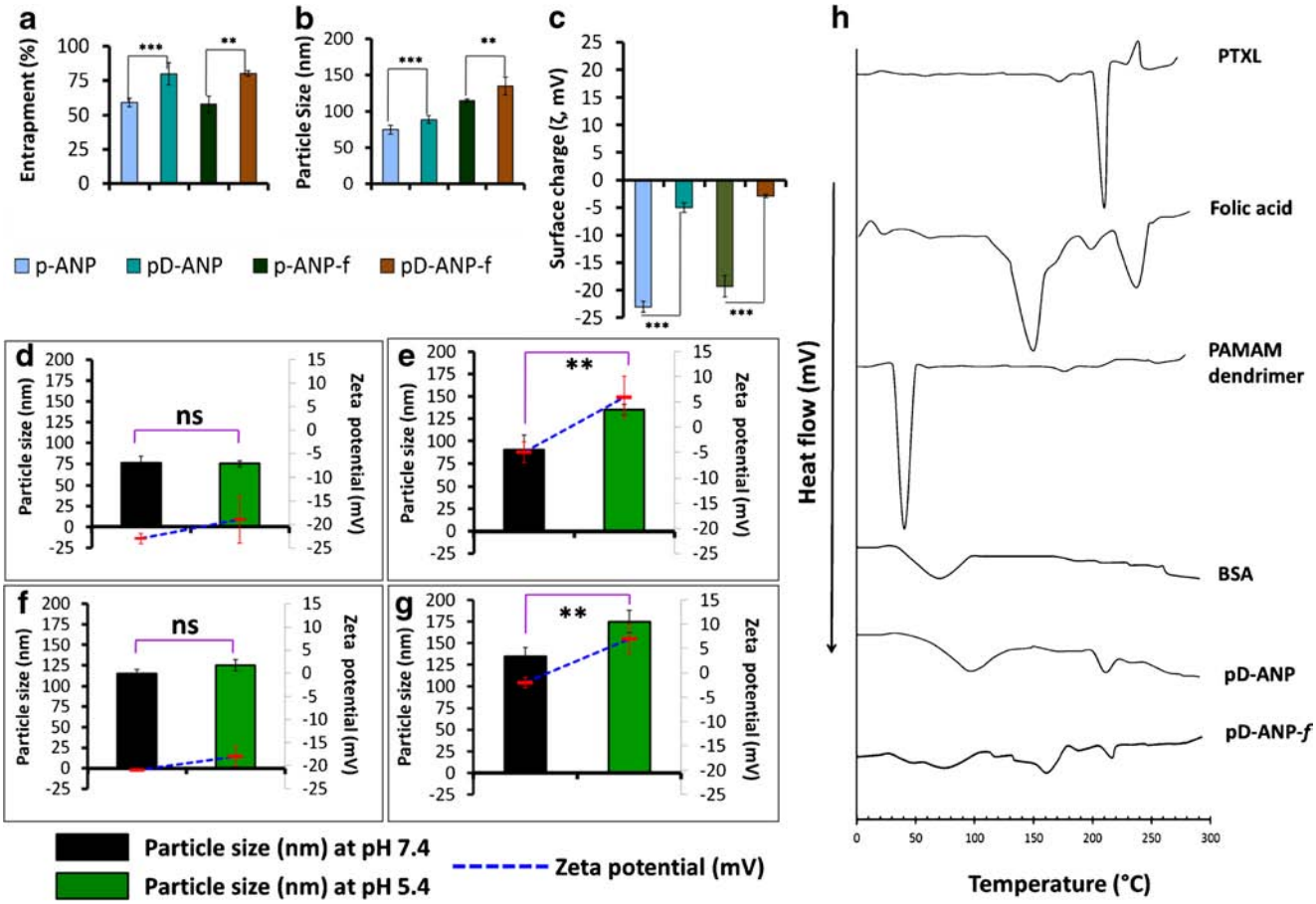

Fig. 4 Figure showing (**a**) Entrapment, %; (**b**) Particle size, nm, and (**c**) Zeta potential, mV of developed nanocarriers. Figure (**d**) p-ANP, (**e**) pD-ANP, (**f**) P-ANP-*f*, and (**g**) pD-ANP-*f* stability of various formulations with respect to particle size (*nm*) and zeta potential (*mV*) under influence of different pH (pH 7.4 and 5.4). DSC thermograms of various nanoformulations are presented in figure (**h**). p-ANP and p-ANP-f represents PTXL loaded non-targeted and folate conjugated ANP's, respectively formulated using conventional method. On the other hand, pD-ANP and pD-ANP-f represents dendrimer stabilized non-targeted and folate targeted ANP's formulated using modified methodology. Results are represented as mean ± SD ($n = 3$). *ns*, non-significant; ***, $P < 0.001$; **, $P < 0.01$,. *, $P < 0.05$.

confirmed the successful folic acid conjugation as well as construction of PTXL-PAMAM coupled targeted albumin nanoparticle (Fig. 6h).

Hemolytic activity

The hemolytic toxicity of plain PTXL, plain PAMAM dendrimer and PAMAM dendrimer-PTXL complex were 19.22 ± 1.01%, 12.71 ± 0.95% and 8.29 ± 0.71%, respectively (Fig. 6). The albumin nanoparticle formulation approach was observed to be a successful move towards producing biocompatible formulation, wherein, p-ANP showed less than 1% hemolytic toxicity. p-ANP-*f* and pD-ANP-*f* also elicited extremely low ($p < 0.005$ in both cases) hemolytic toxicity of 1.29 ± 0.04% and 1.02 ± 0.01%, respectively.

pH stability studies

The pH dependent variation in particle size and surface charge was studied to visualize the transformation in biopharmaceutical properties of developed formulations under physiological (pH 7.4) as well as in tumorous acidic environment (pH 5.4) (7, 41). It was observed that p-ANP and p-ANP-f showed an insignificant ($p > 0.005$) change in particle size on moving from blood physiological to acidic environment; however, minor rise in zeta potential was noticed ($p < 0.05$) (Fig. 4d–f). p-ANP and p-ANP-*f* showed zeta potential of −23.74 mV and −21.93 mV at pH 7.4, nevertheless the incubation of nanoformulations under acidic environment (pH 5.4) leads to notable increment in its surface charge to −19.55 mV and −18.02 mV, respectively).

On the other hand, dendrimer inside the ANP core has potential to change the internal microenvironment with change in pH and ionic strength. Media can penetrate inside the ANP and hence modify protonation of the dendrimer with change in pH and initiate the 'sponge effect' moving outwards and changing the ANP surface environment. Dendrimer stabilized formulation, pD-ANP showed significant ($p < 0.005$) increment in its charge as well as particle size from −5.78 ± 0.31 mV (90.73 ± 11.08 nm) to 6.29 ± 0.44 mV (128.71 ±

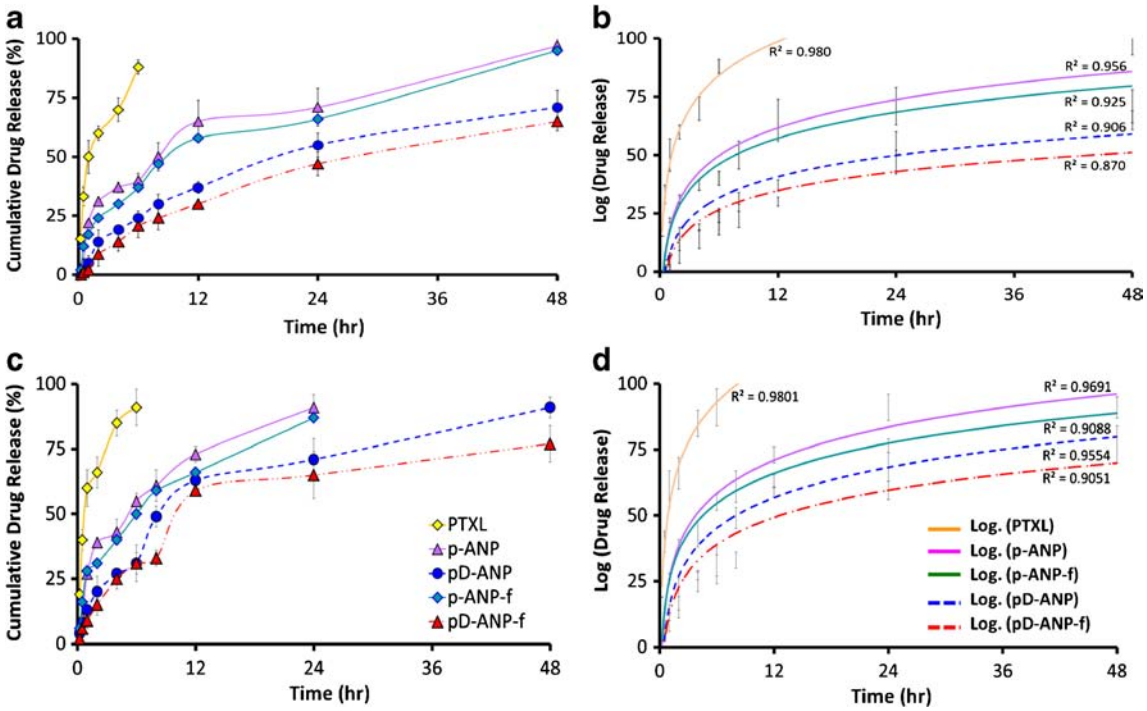

Fig. 5 *In vitro* release profile of PTXL from various nanoformulations under (**a**–**b**) physiological pH 7.4, and (**c**–**d**) under tumoral acidic pH 5.4. Lyophilized nanoformulations were re-suspended in PBS solution and filled inside dialysis membrane cassette (molecular weight cutoff of 12 K Da, Sigma, USA). The dialysis cassette was placed in 500 ml release medium (PBS pH 7.4) maintained at 37 ± 2°Cwith continual slow magnetic stirring (300 rpm). At specific time intervals, 0.5 ml aliquots of dissolution medium was withdrawn and analyzed for PTXL content. Results are represented as Mean ± S.D ($n = 3$).

13.24 nm) while altering the pH from 7.4 to 5.4. Similarly, pD-ANP-*f* also showed significant ($p < 0.005$) rise in its size as well as surface charge from −2.38 ± 0.17 mV (135.08 ± 4.58 nm) to 7.41 ± 0.24 mV (165 ± 7.85 nm) clearly suggesting pH dependent alternation in size/surface charge in case of dendrimer stabilized formulations (Fig. 4d–f).

Cell line based cytotoxicity assay

The outcome of the investigation revealed IC_{50} of PTXL to be 1617.08 ± 52.14 nM, 542.81 ± 39.64 nM, 712.76 ± 12.97 nM, 1,200.69 ± 31.87 nM and 475.05 ± 22.37 nM in SiHa, A549, Jurkat, MCF-7, and HepG2 cell lines, respectively. A slight decrement in IC_{50} of PTXL was noticed following its formulation as p-ANP (1,405.55 ± 29.05 nM, 507.62 ± 16.87 nM, 735.15 ± 13.64 nM, 1,225.91 ± 19.64 nM and 400.82 ± 17.65 nM in SiHa, A549, Jurkat, MCF-7, and HepG2 cell lines, respectively) (Table I).

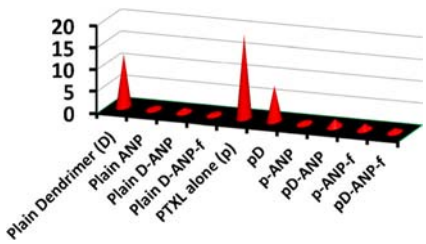

Fig. 6 Hemolytic toxicity profiles of various nanoformulations. p-ANP and p-ANP-f represents PTXL loaded non-targeted and folate conjugated ANP's, respectively formulated using conventional method. On the other hand, pD-ANP and pD-ANP-f represents dendrimer stabilized non-targeted and folate targeted ANP's formulated using method modified methodology. Results are represented as mean ± SD ($n = 3$).

p-ANP-*f* (conventional method driven formulation) also elicited higher cytotoxicity performance (IC_{50}, 1,054.07 ± 23.15 nM, 299.11 ± 20.55 nM, 398.37 ± 11.92 nM, 854.77 ± 31.02 nM and 201.27 ± 15.32 nM in SiHa, A549, Jurkat, MCF-7, and HepG2 cell lines, respectively). However, the most significant reduction in IC_{50} of PTXL was noticed following its delivery by dendrimer stabilized targeted formulation (pD-ANP-*f*) wherein significantly low IC_{50} ($p < 0.005$) of 545.42 ± 17.11 nM, 175.67 ± 14.13 nM, 201.59 ± 10.08 nM, 545.63 ± 18.49 nM and 109.04 ± 9.55 nM was noticed in SiHa, A549, Jurkat, MCF-7, and HepG2 cell lines, respectively (Table I). This clearly indicates that dendrimer stabilization of ANP's further raises the potential of nanocarrier in addition to folate mediated targeting.

Fluorescence and HPLC assay based uptake assay

The outcome of this investigation suggests dendrimer stabilized formulations (^{FITC}pD-ANP/^{FITC}pD-ANP-*f*; Fig. 7c & e) are showing higher level of cell uptake as compared to corresponding nanoformulations produced via conventional method (^{FITC}p-ANP/^{FITC}p-ANP-*f*; Fig. 7b & d). The order of fluorescence uptake following treatment of various FITC

Table I Observed IC_{50} of various PTXL nanoformulations in various cancer cell lines

→Cell lines / ↓Formulations	SiHa		A549		Jurkat		MCF-7		HepG2	
	IC_{50} (nm)	Reduction in IC_{50} (% PTXL)	IC_{50} (nm)	Reduction in IC_{50} (% PTXL)	IC_{50} (nm)	Reduction in IC_{50} (% PTXL)	IC_{50} (nm)	Reduction in IC_{50} (% PTXL)	IC_{50} (nm)	Reduction in IC_{50} (% PTXL)
PTXL	1,617.08 ± 52.14	–	542.81 ± 39.64	–	712.76 ± 12.97	–	1,200.69 ± 31.87	–	475.05 ± 22.37	–
p-ANP	1,405.55 ± 29.05	13.08*	507.62 ± 16.87	6.48*	735.15 ± 13.64	−3.14^{ns}	1,225.91 ± 19.64	−2.10^{ns}	400.82 ± 17.65	15.63*
pD-ANP	1,378.36 ± 75.34	14.76*	416.55 ± 12.91	23.26**	589.22 ± 21.48	17.33*	1,057.02 ± 66.18	11.97*	357.38 ± 12.06	24.77*
p-ANP-*f*	1,054.07 ± 23.15	34.82**	299.11 ± 20.55	44.90**	398.37 ± 11.92	44.11**	854.77 ± 31.02	28.81**	201.27 ± 15.32	57.63***
pD-ANP-*f*	545.42 ± 17.11	66.27***	175.67 ± 14.13	67.64***	201.59 ± 10.08	71.72***	545.63 ± 18.49	54.56***	109.04 ± 9.55	77.05***

For determination of IC_{50} MTT assay was performed using 5×10^3 cells/well by maintaining 96 well plates under condition of 37 ± 0.5°C, 5% CO_2 and 95% humidity. p-ANP and p-ANP-f represents PTXL loaded non-targeted and folate conjugated ANP's, respectively formulated using conventional method. On the other hand, pD-ANP and pD-ANP-f represents dendrimer stabilized non-targeted and folate targeted ANP's formulated using modified methodology. Comparison was made by comparing results between IC50 of PTXL and other groups. Ns; Statistically Non-Significant, *; Significant, **; Very Significant, ***; very-very significant

Negative sign (−) indicates reduction in IC_{50} value

Results are represented as mean ± SD of individual experiments ($n = 3$)

tagged nanoformulations can be concluded as: ^{FITC}pD-ANP-*f* > ^{FITC}p-ANP-*f* > ^{FITC}pD-ANP > ^{FITC}P-ANP > control. The cell uptake of PTXL as assessed by HPLC infers relatively insignificant difference in cellular uptake of PTXL following various nanoformulations, wherein, 0.11 ± 0.003 μg, 0.02 ± 0.001 μg, 0.03 ± 0.001 μg, 0.19 ± 0.003 μg and 0.20 ± 0.001 μg of PTXL per mg cell protein was noted after 0.5 h of formulation treatment ($p > 0.05$) (Fig. 8a). On the other hand, after 8 h, significant enhancement in PTXL uptake was observed with pD-ANP-*f* as compared to p-ANP-*f*. After

Fig. 7 Phase contract and Fluorescence images showing the cell uptake of various FITC tagged nanoformulations viz: (**a** and **f**) Plain FITC treated control, (**b** and **g**) ^{FITC}p-ANP, (**c** and **h**) ^{FITC}pD-ANP, (**d** and **i**) ^{FITC}p-ANP-*f*, and (**e** and **j**) ^{FITC}pD-ANP-*f* formulation treated cells taken after 1 h (at 40× magnification). The samples were imaged using Axiovert 40 CFL inverted microscope at 40× magnification with FITC excitation and emission spectrum peak wavelengths of 495 nm and 519 nm respectively with an Exfo X-Cite series 120 mercury vapor lamp as light source for fluorescence imaging. *Arrow* head indicates interaction of FITC tagged nanoformulations with MCF-7 cells.

8 h, p-ANP-*f* showed 0.72 ± 0.01 µg PTXL per mg cell protein as against to 0.67 ± 0.02 µg PTXL per mg cell protein (Fig. 8a). The outcome of this investigation was in agreement with fluorescence uptake assay.

Caspase-3 activity

The results in Fig. 8b shows that after incubation with untreated control cell group elicited 5.01 ± 0.07 ng caspase-3 per mg of cell protein. Treatment of cells with PTXL showed 23.95 ± 1.12 ng caspase-3, while upon treatment of cells with conventionally targeted albumin nanoparticle 35.05 ± 2.13 ng caspase-3 activity was observed. In an exaggerated manner, significantly higher caspase-3 activity (47.38 ± 1.28 ng/mg cell protein) was observed ($p < 0.01$) pD-ANP-*f* with respect to all other nanoformulations under investigation.

Flow cytometry

The outcome of this investigation suggested 95.18 ± 3.73%, 12.11 ± 0.13%, 42.08 ± 0.95%, 31.61 ± 1.12%, 30.61 ± 0.84% and 19.65 ± 0.42% live cells upon treatment of PBS, plain PTXL, p-ANP, pD-ANP, p-ANP-*f* and pD-ANP-*f* nanoformulations, respectively (Fig. 9a–f). Plain PTXL was found to be an extremely necrosis prone bioactive with 49.97 ± 1.76% necrotic cell population. Treatment of cells with albumin based nanoformulation of PTXL showed reduction in necrotic cell populations with p-ANP, pD-ANP, p-ANP-*f* and pD-ANP-*f* eliciting 30.06 ± 1.17%, 28.19 ± 1.05%, 17.26 ± 0.28% and 9.57 ± 0.02% necrosis. As against to PTXL (39.12 + 0.95% apoptosis), p-ANP and pD-ANP showed 27.09 + 0.33% and 41.77 + 2.02% apoptotic cell population, respectively (Fig. 9c–d). In similar but exaggerated fashion, p-ANP-*f* and pD-ANP-*f* treatment resulted in 51.11 + 1.06% and 73.11 + 3.84% apoptotic cell population, respectively (Figs. 9e–f & 10a).

Tubulin polymerization assay

The PTXL treated cells elicited 19.26 ± 4.97% tubulin polymerization compared to control. The percent tubulin polymerization by p-ANP, pD-ANP, p-ANP-*f* and pD-ANP-*f* was found to be 17.27 ± 3.99%, 25.61 ± 4.01%, 33.16 ± 5.17% and 59.73 ± 6.22%. The % tubulin polymerization was found to be enhanced by 9.82 ± 2.28% and 22.39 ± 4.12% while

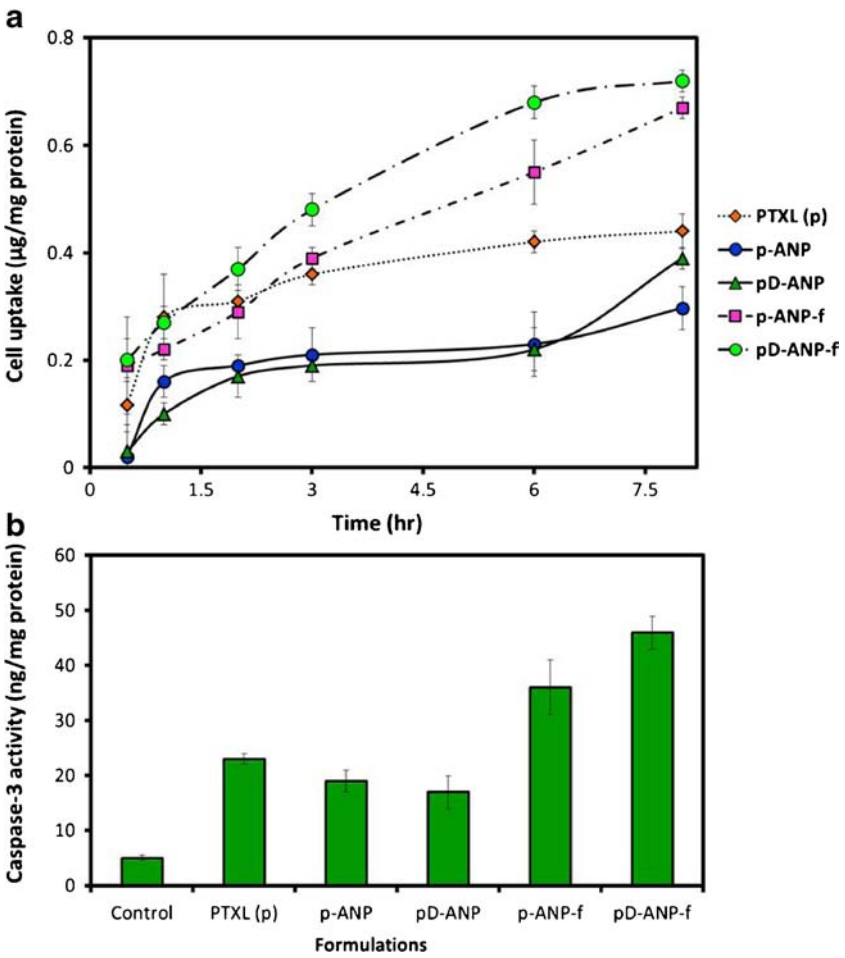

Fig. 8 (**a**) Uptake of PTXL, and (**b**) Caspase activity elicited by MCF-7 cells following treatment of various PTXL nanoformulations at 37 ± 0.5°C. For treatment PTXL concentration in the medium was maintained at 100 nM. p-ANP and p-ANP-f represents PTXL loaded non-targeted and folate targeted ANP's, respectively formulated using conventional method. On the other hand, pD-ANP and pD-ANP-f represents dendrimer stabilized non-targeted and folate conjugated ANP's formulated using method modified methodology. Results are represented as mean ± SD ($n = 3$).

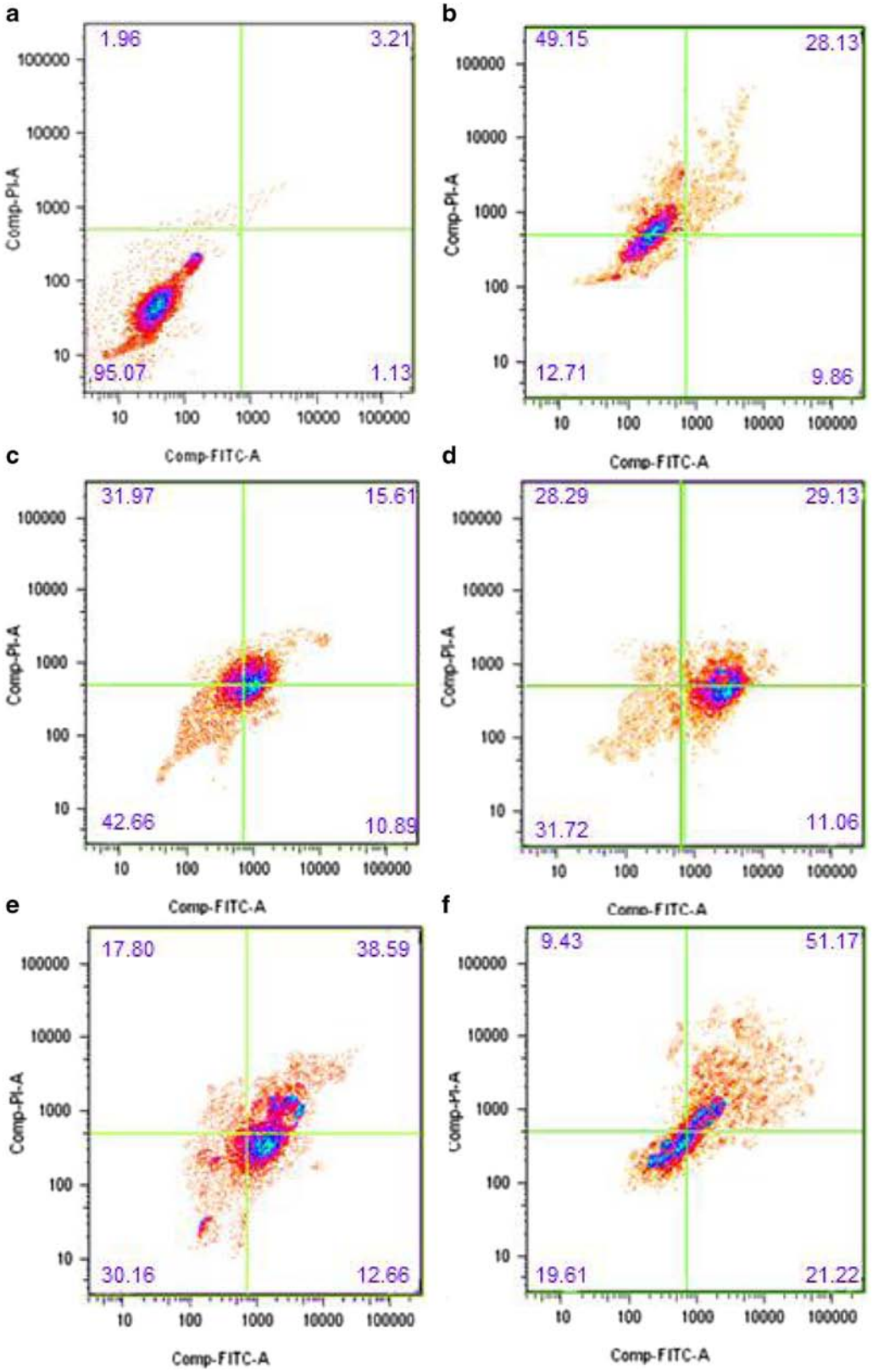

Fig. 9 Annexin-PI flow cytometry evaluation of *MCF-7* cells treated with various PTXL formulations. Untreated control (**a**), Treatment of 100 nM paclitaxel equivalent formulations as (**b**) Plain PTX solution, (**c**) p-ANP, (**d**) pD-ANP, (**e**) p-ANP-f, and (**f**) pD-ANP-f. Control as well as formulation treated cells were incubated with Annexin V-FITC in a buffer containing PI and then flow cytometry was performed on single-cell suspensions by subjecting to fluorescence associated cell sorting (FACS) analysis using FACS ARIA.

stabilizing the passive (pD-ANP) and targeted formulation (pD-ANP-*f*) (Fig. 10b).

DISCUS?SION

With an intention to produce stable albumin nanocarrier with high drug loading as well as sustained and targeted drug release benefit, an innovative strategy of formulation development of stabilized albumin nanoparticles was explored and reported in this investigation. The current research was an extension of our focused research of developing albumin based nanocarrier for successful clinical application (7). The current nanoformulation approach is also expected to progress cationic dendrimer based research that has been stagnant to a great extent owing to toxicity issues related to its surface amino groups (8). The innovative concept of formulation of dendrimer stabilized albumin nanoparticles by encapsulation of drug-dendrimer complex in the core of albumin nanoarchitecture will help in utilizing high loading (10) and sustained release benefit of dendrimer (18) at significantly reduced level of toxicity by masking cationic dendrimers inside biocompatible albumin nanoconstructs (19).

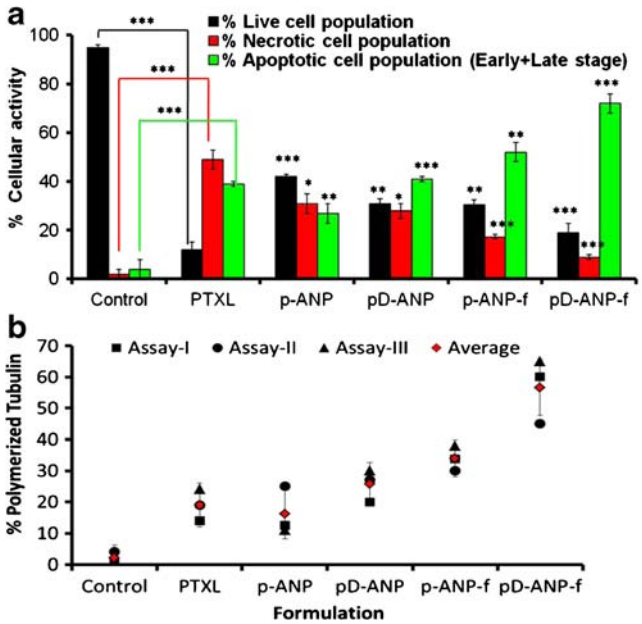

Fig. 10 (**a**) Figure showing the fate (live, apoptotic and necrotic cell population) of MCF-7 cancer cells treated with various PTXL nanoformulations as determined by flow cytometry, (**b**) Effect of various PTXL formulations on tubulin polymerization. p-ANP and p-ANP-f represents PTXL loaded non-targeted and folate targeted ANP's, respectively formulated using conventional method. On the other hand, pD-ANP and pD-ANP-f represents dendrimer stabilized non-targeted and folate conjugated ANP's formulated using modified methodology. In figure 'J' *bullet* represents mean values of three assays. Every time 100 nM PTXL equivalent formulations were used for treatment. Results are represented as mean ± SD ($n = 3$). *ns*, non-significant; ***, $P < 0.001$; **, $p < 0.01$,. *, $P < 0.05$.

As described in the methodology section (Fig. 1), dendrimer stabilized albumin nanoparticles were prepared by ionotropic gelation of the positively charged dendrimer by interaction with negatively charged albumin polymer. Careful analysis of high resolution SEM image (× 50000) inferred dendrimer stabilized formulations (pD-ANP-*f*) to be more rounded, uniformly size distributed as well as stable compared to bulged and non-uniform ANP-*f* formulations formed via traditionally methodology (Fig. 3a–b). As evidenced by TEM microphotographs displayed in Fig. 3c–d, conventionally formed targeted ANP (i.e. p-ANP-*f*) showed rounded/oval shape as against pD-ANP-*f* which were predominantly rounded in shape. Investigation of pD-ANP-*f* at higher magnitude of voltage and magnification clearly inferred existence of dendritic complex in the core of albumin nanoarchitect (Fig. 3e–f).

The slightly larger particle size in case of pD-ANP formulation (89.38 ± 5.62 nm; $p < 0.05$) can be attributed to the encapsulation of drug-dendrimer complex inside the core of ANP as against plain PTXL in case of p-ANP's (75.25 ± 6.91 nm). The particle size distribution curve was found to be more squeezed and constricted in case of pD-ANP than in case of p-ANP (Fig. 2). Also, the polydispersity index in case of p-ANP and pD-ANP was found to be 1.0267 and 0.6205, respectively, which clearly infer dendrimer stabilized ANP formulation to be a superior technique to prepare uniformly sized nanoparticles compared to conventional approach.

The narrow particle size distribution as well as small polydispersity index in case of pD-ANP-*f* (135.17 ± 7.39 nm; PI, 0.1208) compared to p-ANP (115.72 ± 8.69 nm; PI, 0.8358) affirms the capacity of assembling uniformly sized nanoparticles following dendrimer mediated stabilization methodology (Fig. 4a–c).

Conventionally produced p-ANP and p-ANP-*f* showed surface charge of −23.05 ± 1.08 mV and −19.86 ± 2.83 mV, respectively, while the surface charge was found to be amplified (moved towards positivity) by 78.93 ± 5.87% and 89.45 ± 5.02% to yield slightly negative pD-ANP (−5.68 ± 0.95 mV) and pD-ANP-*f* (−2.05 ± 0.37 mV) (Fig. 4a–c). The reduction in surface charge following dendrimer stabilized method was owing to neutralization of negative charge of surface covered albumin (42) by positively charged dendrimer complex (18). The slightly negative charged nanoparticles were reported to be stable and biocompatible with blood components (blood proteins and cells) (43) and will also be helpful in reducing RBC hemolysis which is primarily observed with positively charge nanoformulations (8)

Higher PTXL entrapment was observed in case of pD-ANP and pD-ANP-*f* compared to that of corresponding ANP's. PTXL entrapment in pD-ANP (79.85 ± 8.01%) and pD-ANP-*f* (80.11 ± 4.39%) was found to be 1.33 and 1.50 fold higher compared to p-ANP and p-ANP-*f*, respectively (Fig. 4a–c). The higher entrapment by pD-ANP and pD-

ANP-*f* was attributed to engagement of dendrimer in core, and dendrimer was reported to be loading higher proportion of hydrophobic PTXL in its hydrophobic core by hydrophobic interaction (22). In this case, the loading step involved the interaction between negatively charged albumin polymer (44) and positively charged PTXL-dendrimer complex (22). In case of conventional method lower entrapment efficiency was observed due to unfavorable interaction between negatively charged albumin (44) and negatively charged PTXL (45).

During formulation, the major point of drug loss was found to be the step involving entrapment of PTXL-dendrimer complex inside albumin nanoparticles, wherein approximately 40% PTXL was leaked in case of plain ANPs, while only 20% drug loss was observed while loading was accomplished employing dendrimer stabilization concept (which is one major innovation of this strategy).

The entrapment efficiency of PTXL in pD-ANP was found to be 79.85±8.01%, while after folate anchoring an insignificant change in entrapment efficiency was noted with pD-ANP-*f* (80.11±4.39%; $p>0.005$). This is because folate anchoring was performed in aqueous condition (using water) in which PTXL is insoluble and hence stayed as its loaded form. After folate anchoring, one ml reaction milieu was dried and assayed by HPLC using MeOH:water:TFA acid::80:20:0.1 *v*/*v*/*v* as mobile phase at a flow rate of 1 ml/min, and UV detection at 225 nm at ambient temperature. We did not find any detectable PTXL in the reaction mixture when determined by HPLC.

In vitro release study performed at pH-5.4 suggested that all the ANP formulations under investigation showed pH dependent release profile, but, the effect of pH dependent release was found to be more pronounced in case of dendrimer containing formulations (pD-ANP and pD-ANP-*f*) (Fig. 5b). Both pD-ANP and pD-ANP-*f* showed two phases of initiation of burst release (Fig. 5a–b), with one initiating between 1 and 2 h and the other between 8 and 12 h. This phase of drug release can be attributed to the phase of initial burst release of drug from albumin entangled barrier. While, the second phase of drug associated to albumin as well as dendrimer.

On comparing the release profile at 2 h time point, at pH 7.4 pD-ANP and pD-ANP-*f* released 14.47±1.22% and 8.06±0.17% drug, however, at pH 5.4 same formulations released 20.83±1.75% ($p<0.005$) and 15.97% ($p<0.001$) PTXL, respectively (Fig. 5a). Similarly, when comparing the release profile at 8 h time point, at pH 7.4, pD-ANP and pD-ANP-*f* released 30±2.08% and 24.91% PTXL, while at pH 5.4, same formulations released 49.27% and 33.07% drug, respectively. Similar observations were made at 24 and 48 h time points, which confirm pH dependent release behavior of developed nanoformulations (Fig. 5a–b). This attribute of retaining drug at physiological pH and triggered release of drug under acidic tumoral environment is anticipated to be extremely suitable for drug targeting to tumorous region, where acidic pH exists (46). Although pD-ANP-*f* showed slightly better drug release profile at low pH, more work would be needed to make it fully pH responsive.

During DSC thermal analysis, free PTXL experienced a sharp endothermic peak between 205 and 225°C, which was near the reported melting point of PTXL(≈211°C), while broad endothermic peak ranging from 26 to 55°C was observed in case of plain PAMAM dendrimers. Plain folic acid as well as free BSA showed broad endothermic peaks between temperature ranging 110–190°C and 30–95°C, respectively (Fig. 4h). The DSC curve of PTXL loaded dendrimer stabilized albumin nanoparticle (pD–ANP) showed both the endothermic peaks of PTXL and ANP/PAMAM merged at 203–227°C and 40–130°C, respectively. In the similar line, pD-ANP-*f* showed existence of endothermic peaks of PAMAM, BSA, folic acid and PTXL merged between 40 and 60°C, 60–110°C, 130–180°C and 210–220°C, respectively. These outcomes confirmed the manifestation of successful loading of PTXL inside the dendrimer stabilized albumin nanoconstructs (pD-ANP and pD-ANP-*f*). Similar findings were found in a study by Luppi *et al.*, wherein DSC of BSA as well as BSA nanoparticle was performed (47). Also the existence of shifted as well as slight narrowing endothermic peaks of folic acid in pD-ANP-*f* between 140 and 170°C in place of actual 110–190°C demonstrates the folic acid does not exist in physical mixture but in an intact conjugated form within the dendrimer stabilized pD-ANP-*f* nanoformulation (Fig. 4h).

Hemolytic toxicity assay is a representative of consequence of formulation interaction with blood cells. The outcome of this assay infers PTXL to be a very hemolytic bioactive with 19.22±1.01% hemolysis, irrespective of its very potent anticancer activity (48). The hemolytic toxicity of PTXL-dendrimer complex, pD was found to be 8.29±0.71% suggesting PTXL complex formation to be reducing its toxicity by almost 2.45±0.13 fold. This can be envisaged to the core loading of hydrophobic PTXL inside the hydrophobic core of dendrimer. Also, the surface entangled PTXL covers the peripheral toxic amine groups of dendrimer and generating a complex with reduced hemolytic toxicity. The phenomenon of resulting in less hemolytic dendrimer-drug complex compared to free drug as well as dendrimer was also elucidated in detail by us in our earlier reports. Further, loading of PTXL inside albumin nanoconstructs (p-ANP-*f* and pD-ANP-*f*) leads to an extremely significant reduction in its hemolytic toxicity to 1.29±0.04% and 1.02±0.01%, respectively (Fig. 6). This corresponds to 14.72±0.83 and 11.76±0.95 fold reduction in toxicity of PTXL with p-ANP-*f* and pD-ANP-*f*, respectively. The reduction in hemolytic toxicity by ANP formulations can be envisaged to the extremely biocompatible nature of albumin (4, 42) as is also evinced from negligible hemolytic toxicity of 0.02±0.01% elicited by plain ANP's (placebo).

pH based alternation in surface charge and particle size revealed a sharp increase in surface charge from −2.38± 0.17 mV to 7.41±0.24 mV, while decreasing the incubation pH of pD-ANP-*f* from pH 7.4 to pH 5.4. Similar observation was made in case of dendrimer stabilized non-targeted (pD-ANP) formulations that showed surface charge change from −5.78±0.31 mV to 6.29±0.44 mV (Fig. 4d–g). This corresponds to an increase of surface charge by >200% in both case of pD-ANP and pD-ANP-*f*. This increment in zeta potential in case of pD-ANP and pD-ANP-*f* can be attributed to the pH dependent protonation property of dendrimer (9, 10), which occurs predominantly under acidic condition (tumor pH, where acidic environment subsists).

The increase in surface charge was also found to be accompanied by significant increment in size as is evinced by the size of pD-ANP and pD-ANP-*f* from 90.73±11.08 nm to 128.71±13.24 nm and 135.08±4.58 nm 165±7.85 nm, respectively (Fig. 4d–g). The increment in size of pD-ANP and pD-ANP-*f* upon changing its incubation condition from pH 7.4 to pH 5.4 was found to be 48.03±2.11% and 31.54 ±1.01%, respectively. This increase in particle size can be ascribed to increase in overall charge of ANP's due to protonation of core entrapped dendrimers (8–10). This aspect of eliciting increase in surface charge as well as size of dendrimer stabilized ANP's under acidic conditions is anticipated to be favoring endosomal escape (a key challenge in targeted drug delivery). The rapid release of loaded PTXL in acidic environment as well as slow-sustained release at physiological pH in case of dendrimer stabilized pD-ANP-*f* (Fig. 5a–b) clearly encourages this bioactive to be a smart drug delivery carrier, particular in cancer treatment.

A set of five different cancer cell lines were studied to assess the performance of developed formulations in cancers of different origin and nature. As reported widely (45), PTXL was found to be a potent anticancer analogue with IC_{50} of 1,617.08±52.14 nM, 542.81±39.64 nM, 712.76±12.97 nM, 1,200.69±31.87 nM and 475.05±22.37 nM in SiHa, A549, Jurkat, MCF-7, and HepG2 cell lines, respectively. p-ANP formulation elicited slight reduction in IC_{50} of PTXL by 13.08% ($p<0.05$), 6.48% ($p<0.01$) and 15.63% ($p<0.05$) in SiHa, A549, and HepG2 cell lines, along with a non-significant alternation in IC_{50} of PTXL in Jurkat and MCF-7 cell lines, respectively (Table I). On the other hand, dendrimer stabilized pD-ANP showed notable reduction in IC_{50} of PTXL wherein 14.76% ($p<0.005$), 23.26% ($p<0.001$), 17.33% ($p<0.05$), 11.97% ($p<0.01$) and 24.77% ($p<0.05$) was observed in SiHa, A549, Jurkat, MCF-7, and HepG2 cell lines, respectively. These outcomes clearly infer that inclusion of dendrimer in ANP formulation enhances drug uptake, drug delivery as well as therapeutic potential of loaded PTXL.

The performance of targeted ANP formulations (p-ANP and pD-ANP-*f*) was also studied to evaluate the role of inclusion of dendrimer in ANP formulation as well as its anticancer performance. p-ANP elicited reduction in IC_{50} value of PTXL by 34.82% ($p<0.05$), 44.90% ($p<0.05$), 44.11% ($p<0.001$), 28.81% ($p<0.05$) and 57.63% ($p<0.005$), however, the fall in IC_{50} was found to be more pronounced in case of pD-ANP-*f* by 66.27% ($p<0.005$), 67.64% ($p<0.005$), 71.72% ($p<0.005$), 54.56% ($p<0.005$) and 77.05% ($p<0.005$) in SiHa, A549, Jurkat, MCF-7, and HepG2 cell lines, respectively.

Low anticancer efficacy of p-ANP-*f* compared to pD-ANP-*f* can be attributed to very high negative charge carried by p-ANP (> −20 mV; Fig. 4a–c), which may have hindered the interaction of nanoparticle with negatively charged cell (8). The higher cell kill as well as lowered IC_{50}'s in case of pD-ANP-*f* can be attributed to the combined outcome of folate based targeted delivery of drug as well as dendrimer effect (high protonation, proton sponge effect, rapid drug release, at endosomal pH) (22). Hence, the inclusion of dendrimer in ANP formulation can be stated to be an affirmative move in relation to intratumoral delivery of anticancer drug. Additionally, fluorescence uptake as well as Annexin-PI assay was also performed to closely analyze the anticancer performance of various nanoformulations.

The outcome of fluorescence uptake assay inferred ^{FITC}p-ANP to be eliciting very low cell associated fluorescence as evinced by yellow arrow heads in Fig. 5g. Figure 5h corresponds to fluorescence image of ^{FITC}pD-ANP formulation treated cells, wherein pink arrows clearly shows high cell surface associated fluorescence suggesting pD-ANP's to be primarily localized on the surface of cells.

^{FITC}p-ANP-*f* showed cell surface (primarily) as well as intracellular compartment (minor) associated fluorescence (Fig. 5i), which can be attributed to the folate mediated uptake of nanoformulations. On the other hand, dendrimer stabilized targeted nanoformulations (^{FITC}pD-ANP-*f*) elicited higher cell surface as well as intracellular compartment associated fluorescence (Fig. 5j, red arrow head) owing to existence of surface anchored folate ligand as well as entrapped dendrimer complex that had transformed it into a positive charged nanoconstruct, thereby enabled easy communication with negatively charged cell surface (Fig. 4a–c). Results of our investigation strongly support dendrimer stabilized nanoparticles to be efficient in delivering drugs to tumor cell.

The time dependent cellular uptake of PTXL in MCF-7 cells was assessed following treatment of various nanoformulations using HPLC analysis of cell associated PTXL using method recently reported by our group. The outcome of this investigation infers PTXL to be eliciting time dependent uptake. The uptake of PTXL was found to be higher than p-ANP and pD-ANP, which can be attributed to the ready availability of free PTXL in its naked treatment form as against slow release from passively up taken formulation. It may be noted that both p-ANP and pD-ANP are negatively charged formulations and this negative charge on nanoformulations further impeded their cellular uptake by

negatively charged cell surface. The uptake of PTXL was observed to be higher following its treatment with p-ANP-*f* and pD-ANP-*f* formulations (Fig. 8a). Among these two ligand targeted nanoformulations, uptake was found to be higher in case of pD-ANP-*f*. This might be due to the folate mediated targeting as well as less negative charge of pD-ANP-*f* compared to other albumin nanoformulations under investigation that have high negative charge (Fig. 4a–c). The outcomes of fluorescence uptake assay were in well agreement with HPLC based cellular uptake investigation.

Caspase-3 is an effector caspase that elicits a decisive role in cell apoptosis (programmed cell death). PTXL has been well reported to be inducing apoptosis of cancer cells by inducing caspase-3 activity. To investigate whether nanoformulation based delivery of PTXL could amend the caspase-3 activity of PTXL. pD-ANP-*f* increased the caspase-3 activity most significantly compared with other nanoformulations ($p<0.001$) (Fig. 8b), which was consistent with the observed fluorescence uptake results in Fig. 7j inferring the robust cellular uptake of pD-ANP-*f*.

Further, flow cytometry was also employed to investigate the fate of cells upon treatment with various nanoformulations. Untreated control groups showed existence of more than 95% live cells with less stressed cells ($2.01\pm0.07\%$ necrotic; $3.94\pm0.08\%$ apoptotic population; Fig. 9a). Treatment of cells with plain PTXL formulation resulted in significant reduction in live cells ($12.11\pm0.13\%$), however stressed cells comprised primarily necrotic ($49.97\pm1.76\%$) population (Fig. 9b). p-ANP formulation improved the performance of loaded PTXL, whereupon the necrotic cell population reduced significantly ($30.06\pm1.17\%$, $p<0.05$; Fig. 9c). This effect was probably because of sustained and controlled release of PTXL (44) delivered via biocompatible albumin polymer (7). Similar observations were noted by earlier investigators (49).

The necrotic population was found to be further reduced upon delivering the PTXL employing dendrimer stabilized nanoparticles (pD-ANP), wherein $28.19\pm1.05\%$ necrotic populations were observed (Fig. 9d). This suggests that inclusion of dendrimer leads to slow and sustained availability of PTXL causing enhancement in its anticancer potential ($41.77\pm2.08\%$ apoptosis) as well as reduction in PTXL toxicity ($21.99\pm0.52\%$ less necrosis compared to plain PTXL, $p<0.005$). Similar inference can be drawn from higher proportion of apoptotic cell population observed in case of pD-ANP ($41.39\pm1.05\%$) compared to p-ANP formulation ($27.12\pm0.09\%$, $p<0.005$; Figs. 9c–d and 10a).

Targeting of PTXL was observed to be most eminent strategy to deliver PTXL in cancer treatment. PTXL delivered via p-ANP formulation resulted in further reduction in undesired necrotic cell population ($17.26\pm0.28\%$, $p<0.001$) with parallel rise in apoptotic cell population ($p<0.005$; (Figs. 9c and 10a). However, the most promising observation wasmade in case of dendrimer stabilized targeted nanoformulations, wherein, live and apoptotic cell population was found to be $19.65\pm0.42\%$ and $73.11\pm3.84\%$, respectively. Also, the necrotic cell population reduced significantly to $9.83\pm0.04\%$ inferring pD-ANP-*f* nanoconstruct as a viable strategy in delivering the PTXL to cytosolic environment. pD-ANP-*f* leads to $21.07\pm0.12\%$ (≈1.63 fold) and $9.57\pm0.02\%$ (≈2.13 fold) reduction in cell viability and necrotic cell population, respectively (Figs. 9f and 10a). Also, a $21.73\pm1.18\%$ (≈1.44 fold) enhancement in apoptotic cell population was also observed in case of pD-ANP-*f* compared to p-ANP-*f* ($p<0.05$).

These outcomes are in agreement with our cell line based cytotoxicity assay; however, to examine further the influence of these formulations on mechanistic activity (tubulin polymerization) of PTXL, tubulin polymerization assay was also performed. To investigate the tubulin inhibition efficiency of various PTXL formulations, levels of polymerized and unpolymerized tubulin was determined following treatment of various formulations (Fig. 10b). In case of untreated group, the intrinsic level of polymerized tubulin was found to be $1.95\pm0.05\%$, while a significant rise in the fraction of polymerized tubulin was observed in case of was plain PTXL formulation ($19.26\pm4.97\%$, $p<0.001$). Upon delivering PTXL as conventional nanoparticle formulation (p-ANP) an insignificant amendment in tubulin polymerization ($17.27\pm3.99\%$) was noted compared to plain PTXL formulation ($p>0.05$). This insignificant tubulin inhibition activity noted with p-ANP was probably due to negative charge possessed by this nanoformulation (23.05 ± 1.08 mV; Fig. 4a–c) that might had made its interaction difficult with negatively charged cell membrane.

Upon treating the cells with pD-ANP (-5.68 ± 0.95 mV, Fig. 4a–c), $25.61\pm4.01\%$ polymerized tubulin was observed (Fig. 10b). The enhancement in tubulin inhibition activity was probably because of slightly positive charge possessed by the pD-ANP formulations. Targeted delivery of PTXL elicited most significant enhancement in tubulin polymerization, wherein, p-ANP-*f* and pD-ANP-*f* resulted in $33.16\pm5.17\%$ ($p<0.005$) and $59.73\pm6.22\%$ ($p<0.001$) tubulin polymerization (Fig. 10b). On comparing the tubulin efficacy of p-ANP-*f* and pD-ANP-*f*, $23.82\pm6.28\%$ higher tubulin polymerization ($p<0.001$) was observed in case of dendrimer stabilized targeted nanoformulation (pD-ANP-*f*) compared to that of p-ANP-*f* (Fig. 10b). This effect can be ascribed to the effective targeted delivery of PTXL in the intracellular compartment of MCF-7 cells owing to pH sensitive endosomal escape as well as proton sponge effect (dendrimer mediated) observed in case of dendrimer stabilized nanoformulation (Fig. 4d–g).

CONCLUSION

Previously, our laboratory reported the successful delivery of a variety of drugs based on dendrimeric nanosystems. However,

in spite of extensive applicability of dendrimers in biomedical field, the usage of cationic dendrimers in biosystems is largely constrained owing to inherent toxicity elicited by peripheral amine groups of dendrimers. This work reports formulation of self-assembled nanostructure developed upon controlled electrostatic gelation of anionic bovine serum containing 4.0G PAMAM dendrimer to form supramolecular nano assembly. The outcomes of this investigation are promising for the development of safe nanoformulation which efficiently inhibits the growth of cancer cells of vivid origin compared to plain PTXL as well as conventionally reported albumin nanocarriers. Remarkably, the treatment of pD-ANP-*f* with cancer cells showed noteworthy enhancement in cell associated fluorescence as well as uptake of PTXL as compared to that of unmodified as well as conventionally produced nanocarriers. Based on this investigation, it can be stated that DSSN platform can be successfully employed to accomplish cytosolic delivery of loaded drugs and to attain high intracellular drug concentration. Further it is projected that upon appropriate amendments this technique can be extended to deliver anticancer bioactives of vivid nature, type and origin ranging from drugs, peptides, proteins to genes and siRNA, miRNA etc. It is anticipated that complete exploration of this research will help in translating the use of developed nanocarriers into clinical practice, provided satisfaction of all regulatory concerns.

ACKNOWLEDGMENTS AND DISCLOSURES

RKT acknowledges Commonwealth Scholarship Commission. London (U.K) for the award of Commonwealth Fellowship, and CSIR (New Delhi, India) for providing SRF. MT would like to acknowledge academic staff of TIT COP (Bhopal, India) and SRCP (Bhopal, India) for extending facilities for formulation development and evaluation. We would like to thank Prof. Armin Gerhardt, School of Pharmacy, Concordia University Wisconsin for proof- reading and valuable comments. There is no conflict of interest and disclosures associated with the manuscript.

REFERENCES

1. Bertrand N, Wu J, Xu X, Kamaly N, Farokhzad OC. Cancer nanotechnology: the impact of passive and active targeting in the era of modern cancer biology. Adv Drug Deliv Rev. 2014;66:2–25.
2. Drbohlavova J, Chomoucka J, Adam V, Ryvolova M, Eckschlager T, Hubalek J, *et al.* Nanocarriers for anticancer drugs–new trends in nanomedicine. Curr Drug Metab. 2013;14:547–64.
3. Dawidczyk CM, Kim C, Park JH, Russell LM, Lee KH, Pomper MG, *et al.* State-of-the-art in design rules for drug delivery platforms: lessons learned from FDA-approved nanomedicines. J Control Release: Off J Control Release Soc. 2014;187C:133–44.
4. Bae S, Ma K, Kim TH, Lee ES, Oh KT, Park ES, *et al.* Doxorubicin-loaded human serum albumin nanoparticles surface-modified with TNF-related apoptosis-inducing ligand and transferrin for targeting multiple tumor types. Biomaterials. 2012;33:1536–46.
5. Sethi A, Sher M, Akram MR, Karim S, Khiljee S, Sajjad A, *et al.* Albumin as a drug delivery and diagnostic tool and its market approved products. Acta Pol Pharm. 2013;70:597–600.
6. R. Fanciullino, J. Ciccolini, and G. Milano. Challenges, expectations and limits for nanoparticles-based therapeutics in cancer: A focus on nano-albumin-bound drugs. Critical reviews in oncology/hematology (2013).
7. Tekade RK, Chougule MB. Formulation development and evaluation of hybrid nanocarrier for cancer therapy: taguchi orthogonal array based design. BioMed Res Int. 2013;2013:712678.
8. Tekade RK, Kumar PV, Jain NK. Dendrimers in oncology: an expanding horizon. Chem Rev. 2009;109:49–87.
9. Tekade RK, Dutta T, Tyagi A, Bharti AC, Das BC, Jain NK. Surface-engineered dendrimers for dual drug delivery: a receptor up-regulation and enhanced cancer targeting strategy. J Drug Target. 2008;16:758–72.
10. Tekade RK, Dutta T, Gajbhiye V, Jain NK. Exploring dendrimer towards dual drug delivery: pH responsive simultaneous drug-release kinetics. J Microencapsul. 2009;26:287–96.
11. Mody N, Tekade RK, Mehra NK, Chopdey P, Jain NK. Dendrimer, liposomes, carbon nanotubes and PLGA nanoparticles: one platform assessment of drug delivery potential. AAPS PharmSciTech. 2014;15:388–99.
12. Zidovska A, Evans HM, Ewert KK, Quispe J, Carragher B, Potter CS, *et al.* Liquid crystalline phases of dendritic lipid-DNA self-assemblies: lamellar, hexagonal, and DNA bundles. J Phys Chem B. 2009;113:3694–703.
13. Khopade AJ, Shenoy DB, Khopade SA, Jain NK. Phase structures of a hydrated anionic phospholipid composition containing cationic dendrimers and pegylated lipids. Langmuir: ACS J Surf Colloids. 2004;20:7368–73.
14. Khopade AJ, Caruso F, Tripathi P, Nagaich S, Jain NK. Effect of dendrimer on entrapment and release of bioactive from liposomes. Int J Pharm. 2002;232:157–62.
15. Bitan-Cherbakovsky L, Libster D, Aserin A, Garti N. Complex dendrimer-lyotropic liquid crystalline systems: structural behavior and interactions. J Phys Chem B. 2011;115:11984–92.
16. Khopade AJ, Caruso F. Stepwise self-assembled poly(amidoamine) dendrimer and poly(styrenesulfonate) microcapsules as sustained delivery vehicles. Biomacromolecules. 2002;3:1154–62.
17. Tomita S, Sato K, Anzai J. Layer-by-layer assembled thin films composed of carboxyl-terminated poly(amidoamine) dendrimer as a pH-sensitive nano-device. J Colloid Interface Sci. 2008;326:35–40.
18. Chauhan AS, Jain NK, Diwan PV, Khopade AJ. Solubility enhancement of indomethacin with poly(amidoamine) dendrimers and targeting to inflammatory regions of arthritic rats. J Drug Target. 2004;12:575–83.
19. Thiagarajan G, Greish K, Ghandehari H. Charge affects the oral toxicity of poly(amidoamine) dendrimers. Eur J Pharm Biopharm: Off J Arbeitsgemeinschaft fur Pharmazeutische Verfahrenstechnik eV. 2013;84:330–4.
20. Fischer CR, Groehn V, Reber J, Schibli R, Ametamey SM, Muller C. Improved PET imaging of tumors in mice using a novel (18) F-folate conjugate with an albumin-binding entity. Mol Imaging Biol. 2013; 15:649-54.
21. Jain S, Mathur R, Das M, Swarnakar NK, Mishra AK. Synthesis, pharmacoscintigraphic evaluation and antitumor efficacy of methotrexate-loaded, folate-conjugated, stealth albumin nanoparticles. Nanomed (London, England). 2011;6:1733–54.
22. Khandare JJ, Jayant S, Singh A, Chandna P, Wang Y, Vorsa N, *et al.* Dendrimer versus linear conjugate: Influence of polymeric

architecture on the delivery and anticancer effect of paclitaxel. Bioconjug Chem. 2006;17:1464–72.
23. Tekade RK, D'Emanuele A, Elhissi A, Agrawal A, Jain A, Arafat BT, Jain NK. Extraction and RP-HPLC determination of taxol in rat plasma, cell culture and quality control samples. J Biomed Res. 2013; 27:394-405.
24. Kesharwani P, Tekade RK, Jain NK. Generation dependent cancer targeting potential of poly(propyleneimine) dendrimer. Biomaterials 2014; 35:5539-5548.
25. Thakur S, Tekade RK, Kesharwani P, Jain NK. The effect of polyethylene glycol spacer chain length on the tumor-targeting potential of folate-modified PPI dendrimers. J. Nanopart. Res. 2013; 15:1-16.
26. Dhakad RS, Tekade RK, Jain NK. Cancer Targeting Potential of Folate Targeted Nanocarrier under Comparative Influence of Tretinoin and Dexamethasone. Curr. Drug Delivery 2013; 10:477-491.
27. Ma DH, Lai JY, Cheng HY, Tsai CC, Yeh LK. Carbodiimide cross-linked amniotic membranes for cultivation of limbal epithelial cells. Biomaterials. 2010;31:6647–58.
28. Chougule MB, Padhi BK, Jinturkar KA, Misra A. Development of dry powder inhalers. Recent Patents Drug Deliv Formulation. 2007;1:11–21.
29. Grenha A, Remunan-Lopez C, Carvalho EL, Seijo B. Microspheres containing lipid/chitosan nanoparticles complexes for pulmonary delivery of therapeutic proteins. Eur J Pharma Biopharm: Off J Arbeitsgemeinschaft fur Pharmazeutische Verfahrenstechnik eV. 2008;69:83–93.
30. Ramos-Ninoand ME, Littenberg B. A novel combination: ranpirnase and rosiglitazone induce a synergistic apoptotic effect by down-regulating Fra-1 and Survivin in cancer cells. Mol Cancer Ther. 2008;7:1871–9.
31. Dwivedi P, Tekade RK, Jain NK. Nanoparticulate carrier mediated intranasal delivery of insulin for the restoration of memory signaling in Alzheimer's disease. Curr Nanosci. 2013;9:46–55.
32. Pi J, Jin H, Liu R, Song B, Wu Q, Liu L, *et al.* Pathway of cytotoxicity induced by folic acid modified selenium nanoparticles in MCF-7 cells. Appl Microbiol Biotechnol. 2013;97:1051–62.
33. H. Kong, L. Tao, K. Qi, Y. Wang, Q. Li, J. Du, and Z. Huang. Thymidine kinase/ganciclovir and cytosine deaminase/5-fluorocytosine suicide gene therapy-induced cell apoptosis in breast cancer cells. Oncology reports (2013).
34. Casciola-Rosen L, Rosen A, Petri M, Schlissel M. Surface blebs on apoptotic cells are sites of enhanced procoagulant activity: implications for coagulation events and antigenic spread in systemic lupus erythematosus. Proc Natl Acad Sci U S A. 1996;93:1624–9.
35. van Engeland M, Ramaekers FC, Schutte B, Reutelingsperger CP. A novel assay to measure loss of plasma membrane asymmetry during apoptosis of adherent cells in culture. Cytometry. 1996;24:131–9.
36. Raynaland P, Pollard HB. Annexins: the problem of assessing the biological role for a gene family of multifunctional calcium- and phospholipid-binding proteins. Biochim Biophys Acta. 1994;1197: 63–93.
37. Verrills NM, Po'uha ST, Liu ML, Liaw TY, Larsen MR, Ivery MT, *et al.* Alterations in gamma-actin and tubulin-targeted drug resistance in childhood leukemia. J Natl Cancer Inst. 2006;98:1363–74.
38. Don S, Verrills NM, Liaw TY, Liu ML, Norris MD, Haber M, *et al.* Neuronal-associated microtubule proteins class III beta-tubulin and MAP2c in neuroblastoma: role in resistance to microtubule-targeted drugs. Mol Cancer Ther. 2004;3:1137–46.
39. Chandrasekar D, Sistla R, Ahmad FJ, Khar RK, Diwan PV. Folate coupled poly(ethyleneglycol) conjugates of anionic poly(amidoamine) dendrimer for inflammatory tissue specific drug delivery. J Biomed Mater Res Part A. 2007;82:92–103.
40. Singh P, Gupta U, Asthana A, Jain NK. Folate and folate-PEG-PAMAM dendrimers: synthesis, characterization, and targeted anticancer drug delivery potential in tumor bearing mice. Bioconjug Chem. 2008;19:2239–52.
41. Youngren SR, Tekade RK, Gustilo B, Hoffmann PR, Chougule MB. STAT6 siRNA matrix-loaded gelatin nanocarriers: formulation, characterization, and Ex vivo proof of concept using adenocarcinoma cells. BioMed Res Int. 2013;2013:858946.
42. Wagner S, Rothweiler F, Anhorn MG, Sauer D, Riemann I, Weiss EC, *et al.* Enhanced drug targeting by attachment of an anti alphav integrin antibody to doxorubicin loaded human serum albumin nanoparticles. Biomaterials. 2010;31:2388–98.
43. Ge Y, Zhang Y, Xia J, Ma M, He S, Nie F, *et al.* Effect of surface charge and agglomerate degree of magnetic iron oxide nanoparticles on KB cellular uptake *in vitro*. Colloids Surf B: Biointerfaces. 2009;73: 294–301.
44. Lin W, Garnett MC, Davis SS, Schacht E, Ferruti P, Illum L. Preparation and characterisation of rose Bengal-loaded surface-modified albumin nanoparticles. J Control Release: Off J Control Release Soc. 2001;71:117–26.
45. Wei W, Lv PP, Chen XM, Yue ZG, Fu Q, Liu SY, *et al.* Codelivery of mTERT siRNA and paclitaxel by chitosan-based nanoparticles promoted synergistic tumor suppression. Biomaterials. 2013;34:3912–23.
46. Teow HM, Zhou Z, Najlah M, Yusof SR, Abbott NJ, D'Emanuele A. Delivery of paclitaxel across cellular barriers using a dendrimer-based nanocarrier. Int J Pharm. 2013;441:701–11.
47. Luppi B, Bigucci F, Corace G, Delucca A, Cerchiara T, Sorrenti M, *et al.* Albumin nanoparticles carrying cyclodextrins for nasal delivery of the anti-Alzheimer drug tacrine. Eur J Pharma Sci: Off J Eur Fed Pharma Sci. 2011;44:559–65.
48. Zagouri F, Sergentanis TN, Chrysikos D, Filipits M, Bartsch R. Taxanes for ovarian cancer during pregnancy: a systematic review. Oncology. 2012;83:234–8.
49. Jahanshahia M, Sanati MH, Babaeia Z. Optimization of parameters for the fabrication of gelatin nanoparticles by the Taguchi robust design method. J Appl Stat. 2008;35:1345–53.